國立陽明交通大學

腦科學研究所

碩士論文

Institute of Brain Science

National Yang Ming Chiao Tung University

Master Thesis

探討新穎SHQ1突變在大腦發育的角色

Investigation of the Mechanisms for Novel SHQ1 Variants in the Pathogenesis of Brain Developmental Disorder

研究生：張芊惠（Chang, Chien-Hui）

指導教授：蔡金吾（Tsai, Jin-Wu）

中華民國一一一年七月

July, 2022

探討新穎 SHQ1 突變在大腦發育的角色

Investigation of the Mechanisms for Novel SHQ1 Variants in the Pathogenesis of Brain Developmental Disorder

研 究 生：張芊惠　　Student：Chien-Hui Chang

指導教授：蔡金吾 博士　　Advisor：Dr. Jin-Wu Tsai

國立陽明交通大學

腦科學研究所

碩士論文

A Thesis
Submitted to Institute of Brain Science
College of Medicine
National Yang Ming Chiao Tung University
in Partial Fulfillment of the Requirements
for the Degree of
Master of Science
in
Brain Science

Taiwan, Republic of China

中華民國 一一一年七月

本研究榮獲財團法人罕見疾病基金會
「第二十三屆罕見疾病博碩士論文獎助學金」獎助
謹於此特別致謝

Acknowledgement

在兩年的碩士生活中，雖然過得忙碌，卻十分愉快及充實，沒有一刻覺得疲勞或是想要放棄，這都要感謝這一路走來提拔與支援我的師長、學長姊、同學及學弟妹，「金金 Lab」這個大家庭真的非常溫馨！

最感謝的莫過於蔡金吾老師，即使老師平時工作繁忙，也會不時關心大家的近況，一句「最近還好嗎？」成為實驗室最常響起的話語，除此之外，老師透過每周的小組討論時間，解答我們在實驗時遇到的瓶頸，並引導專題研究走向，在最後碩士論文修改期間，老師也非常有耐心地教導我如何將實驗結果有邏輯地整理成一篇學術論文，謝謝老師提供這麼優良的研究環境與氛圍，讓我在碩士生活結束之際，滿懷熱忱地想要繼續進行學術研究，探討神經發育的奧妙。

再來要感謝一直以來教導我的博士班學長嘉偉，不管是在實驗、研究方向、報告和生活上都提供了許多建議和協助，並且教導我在埋頭做實驗之餘，要學會停下來思考實驗結果及未來研究走向，此外，學長也會時常提供獎學金、講座和留學的資訊，讓我的研究生活過得十分豐富和精彩。另外，要感謝在我實驗遇到困難時，即使忙碌也會停下來提供援助的學長姊們，謝謝芳馨學姊在我獨自嘗試免疫共沉澱法的條件的時候，幫我想造成問題的可能原因及解決方法，也教我思考如何用不同實驗方法來驗證我們想回答的問題。謝謝皓元學長總是在我報告完研究進度和 paper 後，走到台前跟我分享他的經驗和想法，每次與學長討論過後，就會知道自己的報告還有哪裡需要改進。謝謝佳萱學姊總是幫忙大家配各式各樣的溶液，當我在西方墨點法遇到困難時，學姊也幫我想各種可能的解決方法。謝謝巧玟提供給我許多免疫染色的小撇步，也教我如何操作 tunel assay，還時常關心我有沒有吃飯，聆聽我的煩惱，並且提供建議。

研究生活能夠那麼順利，還要歸功於實驗室助理坤銓、岳儒和 penny，謝謝助理們辛苦地幫忙訂貨、報帳和處理各式雜務，實驗室設備常常壞掉，也是多虧助理們及時處理，才不至於讓樣品壞掉，看到助理們常常因為繁雜的行政事務及實驗忙得焦頭爛額，真的是辛苦你們了！

謝謝你們把實驗室管理的這麼好，才能讓大家無後顧之憂地做實驗。

在研究生活中，也多虧了同學們的陪伴與支持，才能讓我這兩年過得非常歡樂與幸福。謝謝莞茜一開始教了我許多分生實驗，後來也常常和我討論實驗和生活，在我算細胞很累的時候，總會跑來和我聊天和按摩肩膀，讓我能繼續堅持下去。謝謝悠妮總是帶來歡笑，著實是實驗室的開心果，在休息室一邊吃零食一邊聊天、聊夢想，真的是研究生活最快樂的時光，也謝謝在德國的時候，那麼用心地安排、接待和介紹。謝謝從頭到尾都坐在我旁邊的鄰居采諭，總是聽我分享研究生活中發生的有趣事蹟，一起出國參加研討會時，也總是陪伴在身邊。謝謝 Agnes 總是關心大家，在實驗室裡也常常講話逗大家笑，讓氣氛一直都很愉快。謝謝 Dewi 總是笑著跟大家打招呼，並且關心大家的近況，也常常分享好吃的印尼美食。

謝謝在這一路上所有幫助過我的人，希望未來還有機會一起共事！

摘要

背景與目標： SHQ1 是 H/ACA RNPs 組裝的重要調控因子，H/ACA RNPs 參與在許多重要的生物途徑，如核糖體生成、mRNA 剪接及維持端粒長度。當與 H/ACA RNPs 相關的基因發生突變，即會造成先天性角化不全症，病患會有骨髓衰竭症候群及端粒酶活性低下或端粒較短的問題。在本篇研究中，我們找到一位病人在 SHQ1 基因的兩個基因座，分別帶有不同的突變。 病人被診斷出多重神經功能失調，臨床表徵包含發育遲緩、運動障礙、癲癇、以及小頭畸形。因此我們欲探討 SHQ1 於大腦發育過程中的角色。

材料與方法： 為了在胚胎小鼠腦中調控 Shq1 的表現量，我們首先利用子宮內電穿孔將 shRNA 送入小鼠胚胎之神經幹細胞中，並觀察神經細胞的分佈及特性。接著為了闡明 SHQ1 突變的致病機制，我們利用免疫共沉澱法觀察突變型 SHQ1 與 H/ACA RNPs 核心蛋白之間的交互作用。

結果： 我們發現當 Shq1 失去功能時，會導致神經細胞遷移異常，但是並不會影響神經細胞增殖、分化、及凋亡等機制，此外，我們也發現大部分的突變型 SHQ1 與 DKC1 的結合能力會大幅下降，由以上結果我們推測 SHQ1 突變會藉由擾亂 H/ACA RNP 的組裝與生成，進而影響大腦發育。

結論： SHQ1 藉由調控神經先驅細胞及神經細胞的特性以影響大腦的發育。本研究使我們對於 SHQ1 在大腦發育中所扮演的角色有更多的了解，並提供了 H/ACA RNP 相關病症可能的致病機制。

關鍵字：SHQ1、H/ACA RNP、大腦皮質發育、先天性角化不全症

Abstract

Background and Aims: SHQ1 is an assembly factor of H/ACA ribonucleoproteins (H/ACA RNPs) which are involved in many critical biological pathways, including ribosome biogenesis, mRNA splicing and telomere maintenance. Mutations found in H/ACA RNPs components have been reported to cause dyskeratosis congenita (DKC), a genetic disorder characterized by bone marrow failure and poor telomere maintenance. Here, we identified novel SHQ1 compound heterozygous mutations from a patient with multiple neurological disorders, including developmental delay, movement disorders, epilepsy, and microcephaly. In this study, we aim to investigate the potential role of SHQ1 in brain development.

Materials and Methods: To modulate Shq1 expression in developing brains, we introduced short-hairpin RNA (shRNA) into neural progenitors in the embryonic mouse cortex by utilizing in utero electroporation. The distributions and identities of electroporated cells were examined by immunostaining. To elucidate the pathogenic mechanism of SHQ1 mutations, we then performed co-immunoprecipitation to investigate the interaction between SHQ1 and DKC1 which is a core protein of H/ACA RNPs.

Results: We found that decreased Shq1 impaired neuronal migration but may not affect neural progenitor proliferation, neuronal apoptosis, and neuronal differentiation during brain development. In addition, we found that most of SHQ1 variants attenuated their binding ability toward DKC1. These results implied SHQ1 mutations may influence brain development through disrupting the assembly and biogenesis of H/ACA RNPs.

Conclusions: SHQ1 plays an essential role in brain development through regulating the behaviors of neural progenitors and their neuronal progeny. Our study gave a glimpse of the functions of SHQ1 in brain and provided a possible pathogenic mechanism for H/ACA RNPs-related disorders.

Key words: SHQ1, H/ACA RNP, cerebral cortex development, dyskeratosis congenita

Table of Contents

List of Tables

List of Figures

Chapter 1: Introduction

1.1 Cerebral cortex development

Development of the nervous system in vertebrates begins when the neural plate forms from the embryonic ectoderm during the gastrulation stage. The neural plate is then folded and fused to form the neural tube. The rostral part of the neural tube is dilated to form three primary brain vesicles: the forebrain (prosencephalon), the midbrain (mesencephalon), and the hindbrain (rhombencephalon). The forebrain further segregates into two secondary brain vesicles: the telencephalon and the diencephalon. The telencephalon forms the cerebrum and the diencephalon forms the epithalamus, the thalamus, and the hypothalamus (Moore, 2016; Sadler and Langman, 2012).

In mammals, the cerebral cortex develops from the pallium which is the dorsal part of the telencephalon. The development of cerebral cortex in mammals requires highly organized developmental steps. At the beginning of cortical development, neuro-epithelial (NE) cells divide symmetrically to expand the progenitor pool. Meanwhile, some NE cells would transform into radial glial (RG) which located in ventricular zone (VZ) (Noctor et al., 2002). The RG cells are progenitors which can divide asymmetrically to form RG cells and neurons (Noctor et al., 2001). RG cells can also generate intermediate progenitors which will eventually divide symmetrically to produce more neurons in the subventricular zone (SVZ) (Haubensak et al., 2004; Noctor et al., 2004).

The pyramidal projection neurons, the most common cells in the cerebral cortex, undergo elaborate radial migration processes to form the six layers of the cortex. The newly born neurons first exhibit multipolar morphology in the SVZ for about 24hr (Noctor *et al.*, 2004; Tabata and Nakajima, 2003). These neurons further transform into bipolar morphology and migrate along the radial fiber of RG cells to reach the cortical plate (CP) (Nadarajah et al., 2001; Rakic, 1972). The neuronal migrations are

performed in an inside-out manner, by which the earliest generated neurons form the deeper layers of the CP, whereas the latest generated neurons form the upper layers of the CP (Rakic, 1974).

1.2 The maturation of cortical projection neurons

The maturation of pyramidal projection neurons requires three main steps: primary axon extension, delayed collateral branch formation, and selective axon elimination (O'Leary and Koester, 1993). According to the divergent axon projections, pyramidal projection neurons can be classified into three subtypes: corticofugal projection neurons (CFuPN), callosal projection neurons (CPN), and ipsilateral circuit connection neurons. CFuPNs extend their axons away from the cortex to deeper brain areas, the brainstem, or spinal cord. The cell bodies of CFuPNs mainly reside in layers IV and V of the cortex. Conversely, the cell bodies of most CPNs predominantly reside in layer II/III of the cortex; the cell bodies of about 10% of these cells reside in the deep layers V and VI. CPNs can be further classified into 4 major types based on projection patterns: (1) single projection to the contralateral cortex; (2) dual projections to the contralateral cortex and ipsilateral or contralateral striatum; (3) dual projections to the contralateral cortex and ipsilateral premotor cortex; and (4) dual projections to the contralateral cortex and ipsilateral sensorimotor cortex (Cauller et al., 1998; Mitchell and Macklis, 2005; Wilson, 1987).

A variety of molecular controls is required for the maturation processes of pyramidal projection neurons. For example, Satb2 (special AT-rich sequence-binding protein 2), which is mainly expressed in CPNs, is an essential regulator for axon outgrowth of callosal projections (Alcamo et al., 2008; Britanova et al., 2008). Ctip2 (COUP-TF interacting protein 2), mainly expressed in deeper layer neurons, is also a transcription factor regulating the axon outgrowth of subcortical projection (Arlotta et al., 2005).

1.3 Malformation of cortical development

Malformation of cortical development (MCD) is a wide spectrum of disorders due to interference in the processes of cortical development. MCD can result from abnormal cell proliferation, cell migration, and cell organization, depending on the stages when the abnormality occurs during cortical development (Barkovich et al., 1996; Barkovich et al., 2001). The first step of cortical development is cell proliferation in which stem cells keep dividing to expand the progenitor pool. Abnormality at this stage can cause severe defects, such as microcephaly, a developmental disorder characterized with abnormally small brain size (<-3 SDs over mean) due to decreased neural progenitor proliferation and/or increased neuronal apoptosis (Leviton et al., 2002). Toxins, infections, and genetic mutations, such as MCPH1, WDR62, CENPJ, and CEP152, can give rise to microcephaly.

Aberrant neuronal migration can cause lissencephaly, cobblestone complex, and heterotopia. Lissencephaly is characterized by smooth brain with less or absence of gyri. Patients with lissencephaly only have 4-layered cortex: (1) outer marginal layer, (2) superficial cellular layer, (3) cell sparse layer, and (4) deep cellular layer. Mutations in DCX and LIS1 can lead to lissencephaly which results in developmental delay, spastic quadriplegia, and epilepsy (des Portes et al., 1998; Dobyns et al., 1993; Gleeson et al., 1998). Cobblestone complex, characterized with irregular heterotopic tissue on brain surface, results from overmigration of neurons. Patients with cobblestone complex suffer from eye malformation and muscular dystrophy (Dobyns et al., 1985). Heterotopias, a group of mature neurons resided in abnormal brain area, are caused by disturbance of neuronal migration. Patients with heterotopias would usually develop seizure disorder (Battaglia et al., 1997; Dubeau et al., 1995; Raymond et al., 1994).

In later stage of cortical development, normal cortical function requires the maturation of neurons and the extension of neurites. For example, agenesis of corpus callosum (AgCC) results from defects in axonal projection. It can be categorized into type I and type II based on the presence or absence of abnormal fiber bundles along the medial

hemispheric walls, termed the Probst bundles (Schell-Apacik et al., 2008). In type I AgCC, axons can be formed but fail to cross the midline. These uncrossing axons develop into Probst bundles. In contrast, type II AgCC fails to form commissural axons; therefore, no abnormal fiber bundles are observed. Interestingly, isolated AgCC usually does not cause severe symptoms. However, AgCC in combination with other abnormality, such as schizencephaly and holoprosencephaly, often results in epilepsy (Taylor and David, 1998).

1.4 Identification of novel SHQ1 variants

Recently, we discovered a patient with feeding difficulties, dystonia, orofacial dyskinesia, extremities dyskinesia and multiple neurological disorders, including epilepsy, cerebellar atrophy, and microcephaly from National Taiwan University Hospital (Table 1). Using Whole Exome Sequencing (WES), we identified novel SHQ1 compound heterozygous variants, p. Leu333Val (L333V) and p. Tyr65Ter (Y65X), in this patient. These variants were inherited from their heterozygote parents, who did not develop any symptoms, suggesting that the inheritance of this disorder was autosomal recessive (Figure 1a).

The mutation sites were showed on the predicted protein structure of SHQ1 (Alpha fold, AF-Q6PI26-F1) (Figure 1b). The truncated variant Y65X was terminated at the CS (CHORD-containing proteins and SGT1) domain. The missense variant L333V was located at the SS (SHQ1-specific) domain (Figure 1c). Both domains were required for SHQ1 to interact with H/ACA RNP core protein DKC1. However, how SHQ1 variants cause brain developmental defects were largely unknown.

1.5 H/ACA box ribonucleoproteins

H/ACA box ribonucleoprotein (H/ACA RNP) complex consists of RNAs containing

specific sequences of H (ANANNA) and ACA boxes, and their interacting proteins, DKC1, NOP10, NHP2, and GAR1. There are three types of H/ACA box RNAs: small nucleolar RNAs (snoRNAs), small cajal body-specific RNAs (scaRNAs), and telomerase RNAs, depending on their subnuclear localization (Balakin et al., 1996; Darzacq et al., 2002; Ganot et al., 1997; Mitchell et al., 1999). Among these 3 H/ACA RNAs, snoRNAs and scaRNAs direct pseudouridylation, which converts uridine to pseudouridine, of pre-rRNA and spliceosomal RNA respectively (Cohn, 1960; Cohn and Volkin, 1951; Davis and Allen, 1957). The exact function of pseudouridylation is so far unknown. Telomerase RNAs, the third kind of H/ACA RNAs, serve as template RNA during telomere replication for the telomerase to join DNA repeats to maintain telomeric integrity.

The biogenesis of H/ACA RNP requires multiple core proteins and assembly factors. First, SHQ1, an assembly factor, binds with unstable DKC1 in the cytoplasm (Lafontaine et al., 1998; Yang et al., 2002). Next, SHQ1-DKC1 complex shuttles into the nucleoplasm. Other assembly factor NAF1 and core proteins NOP10 and NHP2 are then recruited to DKC1. The protein complex subsequently binds with H/ACA box RNAs to form pre-H/ACA RNP complex. Finally, the pre-H/ACA RNP complex enters Cajal body where NAF1 is replaced by GAR1 to form an active and mature H/ACA RNP complex.

1.6 Dyskeratosis congenita

Dyskeratosis congenita (DC) is a genetic disorder typically characterized by bone marrow failure, skin pigmentation, oral leukoplakia, nail dystrophy, and poor telomere maintenance (Zinsser, 1906; Engman, 1926). Mutations in several genes have been found to account for this disorder, including H/ACA RNP components (DKC1, NAF1, NHP2, NOP10, GAR1), telomerase complex proteins (TERT, TERC, WRAP53, CTC1, RTEL1), and shelterin complex proteins (TRF1,TRF2, RAP1, TIN2, POT1, ACD) (AlSabbagh, 2020). Hoyeraal-Hreidarsson syndrome (HHS), one of the severe forms of DKC, is characterized by intrauterine growth retardation, microcephaly, and

cerebellar hypoplasia (Hoyeraal et al., 1970; Hreidarsson et al., 1988). Patients with HHS do not develop classical skin abnormalities generally due to high early life mortality.

Although many genes related to H/ACA RNP have been reported to cause DC, SHQ1 mutations have not been reported in DC patients. Until now, only five SHQ1-related cases had been reported in the world. One was reported by Bizarro and Meier in 2017. The other four were reported by Sleiman in 2022. All these mutations lie in the heart of the unique SHQ1 specific domain (SSD) which functions as protein-protein interaction sites with DKC1. The pathogenic phenotypes and genotypes of each individual with SHQ1 variants were summarized in Table 1 (Bizarro and Meier, 2017; Sleiman et al., 2022).

1.7 Significance

This study shed light on the roles of SHQ1 in brain development, which may provide potential therapeutic strategies for SHQ1-related disorders. Furthermore, the symptoms of the patients with SHQ1 mutation resemble that of the patients with Hoyeraal-Hreidarsson syndrome. Accordingly, we could include SHQ1 gene screening for diagnosis of Dyskeratosis congenita or idiopathic bone marrow failure syndrome.

Chapter 2: Materials and Methods

2.1 Constructs

SHQ1 shRNAs (shShq1) and scrambled control (shCtrl) inserted to pLKO_TRC005 vectors were acquired from National RNAi Core Facility in Taiwan. The target sequences of shRNAs were as follows: shCtrl: 5’- C C T A A G G T T A A G T C G C C C T C G -3’; shShq1#1: 5’- C T C A A G T G G T G C G C T C A T T A C -3’;

shShq1#2: 5’- A G C C T A C C G A G A C A C T A T A A A -3’; shShq1#3: 5’- C T A T C C A C T T T A T C G T C A T T T -3’; shShq1#4: 5’- T G A G T G A G G T T A T C G A T A T T A -3’. PLKO_TRC005 vector contained PAC gene which produced puromycin acetyltransferase.

To obtain HA-tagged Human SHQ1 cDNAs (SinoBiological, Cat. #: HG23861-NY; NCBI Ref Seq: NM_018130.2) with patient mutations, mutagenesis was performed by using QuikChange Lightning Site-Directed Mutagenesis Kit (Agilent Technologies, Cat. #: 21059). WT and mutant SHQ1 cDNAs were then cloned to pCAGIG vector (Addgene, Cat. #: 11159) by using EcoRI and NotI restriction enzymes in order to express in mouse animal model.

2.2 Cell culture and transfection

To test the knockdown efficiency of shRNAs, mouse neuroblast cell line Neuro-2a (N2a) was used. We cultured N2a cells in Dulbecco’s Modified Eagle Medium (DMEM) supplemented with 10% L-glutamine, 10% Penicillin-Streptomycin (P/S), sodium pyruvate, sodium bicarbonate, and 10% fetal bovine serum (FBS). When N2a cells reached about 70% confluence, cells were transfected with each shRNAs for 24 hours using Lipofectamine 3000 transfection reagent (Invitrogen, Cat. #: L3000075) followed by puromycin selection for 50 hours.

For expressing different SHQ1 variants, human embryonic kidney cell line HEK293T was used due to their highly-transfectable characteristics. We cultured HEK293T cells in Dulbecco’s Modified Eagle Medium (DMEM) supplemented with 10% L-glutamine, 10% Penicillin-Streptomycin (P/S), sodium pyruvate, sodium bicarbonate, and 10% fetal bovine serum (FBS). When HEK293T cells reached about 70% confluence, cells were transfected with each SHQ1 variants for 24 hours.

For protein extraction, cells were lysed by RIPA buffer (50 mM Tris-HCl, pH 8.0, 150

mM NaCl, 1% IGEPAL® CA-630, 0.5% sodium deoxycholate, 0.1% SDS, and 10% protease inhibitor) (Sigma-Aldrich, Cat. #: R0278)

2.3 Animal

Timed pregnant ICR mice were set up under following condition. The morning of vaginal plug appearing represented embryonic (E) day 0.5 of pregnancy. The day of birth represented postnatal (P) day 0.

2.4 *In utero* electroporation (IUE)

In utero electroporation was performed on pregnant ICR mice at E14.5 anesthetized with isoflurane. The plasmids (1.5 μg/μL) were injected into lateral ventricle of embryonic mice brain. Electroporation was performed with a forceps electrode involving five 50ms pulses with an interval of 450ms at a voltage of 50V. Embryos or neonates were perfused with PBS and 4% paraformaldehyde at E16.5, E18.5, and P7. Whole brains were harvested and immersed in 4% paraformaldehyde overnight.

2.5 Immunohistochemistry

Fixed brains were embedded in 4% Agarose II (VMR Life Science, Cat. #: 0815-250G) in Phosphate Buffer Saline (PBS) and sliced coronally at the thickness of 100μm using Vibratome (Leica, VT1000S). Slices were then stored in PBS supplemented with 0.05% sodium azide (VWR, Cat. #: 0639) at 4˚C.

For immunostaining, slices were first permeabilized with PBS supplemented with 0.2% Triton X-100 (Sigma-Aldrich, Cat. #: T8787). Next, slices were blocked with PBS supplemented with 0.2% Triton X-100, 5% BSA (Bovine Serum Albumin) and 10%

NGS (Normal Goat Serum) for 1 hour at room temperature. This was followed by incubating in primary antibodies prepared in blocking buffer (0.2%Triton X-100, 5% BSA, and 5% NGS in PBS) for 3 days at 4˚C. The concentration of primary antibodies that was used: Ki67 (1:500, abcam, Cat. #: ab15580), NeuN (1:500, Merck Millipore, Cat. #: ABN78), Satb2 (1:700, Santa Cruz, Cat. #: sc-81376), and Ctip2 (1:500, Abcam, Cat. #: ab18465). After slices were washed with PBS, secondary antibodies prepared in blocking buffer (0.2% Triton X-100, 2.5% BSA, and 2.5% NGS in PBS) were added to slices for 2 hours at room temperature. Lastly, slices were counterstained with 4',6-Diamidino-2-Phenylindole, Dihydrochloride (Invitrogen, Cat. #: D1306), mounted with VECTASHIELD® Antifade Mounting Medium (Vector Laboratory, Cat. # H-1000), sealed under coverslips with nail polish, and stored at 4˚C.

2.6 TUNEL assay

TUNEL assay was performed using In Situ Cell Death Detection Kit, TMR red (Roche, Cat. #: 12156792910). The TUNEL reaction mixture was prepared freshly on ice before use. Brain slices were fixed, permeabilized, and labeled according to manufacturer's protocol.

2.7 Co-immunoprecipitation

Whole HEK293T cell lysates transfected with HA-tagged WT or mutant SHQ1 cDNAs were harvested using cell lysis buffer (20 mM Tris-HCl, 150 mM NaCl, 2 mM EDTA, 0.4% NP-40, and 10% protease inhibitor). Cell lysates were constantly agitated on rotor for 1hr at 4˚C and were centrifuged at 20,000xg for 10 minutes. Supernatants were collected and quantified by Pierce BCA Protein Assay Kit (Thermo Fisher Scientific, Cat. #: 23225).

Anti-HA tag antibodies (abcam, Cat. #: ab9110) were incubated with PureProteome™

Protein G Magnetic Beads (Merck Millipore, Cat. #: LSKMAGG02). After washing with PBS supplemented with 0.02% Tween-20, bead-antibody complex was resuspended with 400μg of whole cell lysates. To elute target proteins, 1X sample dye was added to bead-antibody-antigen complex. Samples were heated at 95˚C for 10 minutes.

2.8 Western blotting

Protein samples (50μg/lane) were separated on 10% or 4-20% SDS-PAGE. The separated samples were then transferred to 0.45μm or 0.22μm pore size PVDF (Polyvinylidene Difluoride) membranes with Tank Transfer System (Bio-Rad). Membranes were blocked in blocking buffer (5% non-fat milk in 0.1% TBST buffer) for 1 hour at room temperature and were incubated in primary antibodies prepared in blocking buffer overnight at 4°C. The concentration of primary antibodies that was used: Shq1 (1:1000, Novus Biologicals, Cat. #: NBP2-81793), SHQ1 (1:1000, Proteintech, Cat. #: 27020-1-AP), GAPDH (1:10000, Proteintech, Cat. #: 60004-1-Ig), HA (1:2000 for WB, 1:100 for Co-IP, Proteintech, Cat. #: 66006-1-Ig), and DKC1 (1:200, Santa Cruz, Cat. #: sc-373956). After membranes were washed with 0.1% TBST buffer for 10 minutes three times, membranes were incubated in secondary antibodies (goat anti-mouse IgG-HRP or goat anti-rabbit IgG-HRP) diluted in blocking buffer for 1 hour at room temperature. The probed membranes were detected by Enhanced Chemiluminescence HRP substrate reagent and visualized by Luminescence Image System LAS-4000. The signal was quantified by Image-J software.

2.9 Quantitative reverse transcription PCR (RT-qPCR)

Total RNA was isolated from cells by TOOLSmart RNA Extractor (Cat. #: DPT-BD24). Total RNA was then converted into cDNA by RT-PCR using FIREScript RT cDNA Synthesis MIX with Oligo (dT) and Random primers (Solis BioDyne, Cat. #: 06-20-00100). Lastly, qPCR reaction mix was prepared using 5 x HOT FIREPol® EvaGreen®

qPCR Mix Plus (ROX) (Solis BioDyne, Cat. #: 08-24-00001). The qPCR reaction was set up using StepOnePlus™ Real-Time PCR System (Applied Biosystems, Cat. #: 4376600). $2^{-\Delta\Delta CT}$ method was used to analyze the relative mRNA level. The following primers were used for qPCR: Shq1 forward, 5'- G C T A G A C A A G A C G G C T C A C C -3' and reverse, 5'- A T T C A A C G C T G T G C T C T C C T -3'; Gapdh forward, 5'- T G A A C G G G A A G C T C A C T G G -3' and reverse, 5'- T C C A C C A C C C T G T T G C T G T A -3'.

2.10 Image analysis

Confocal microscopy (ZEISS LSM700) was used to obtain images. ImageJ software was used to calculate cell distribution and colocalization of different markers in the cortex.

Chapter 3: Results

3.1 Shq1 loss-of-function altered neuronal cell distribution in developing mouse cortex

To investigate the potential role of Shq1 in brain development, we first examined the expression of Shq1 in the developing mouse cortex. We collected mouse cortices at different stages from embryonic (E) day 13.5 to postnatal (P) day 30 and analyzed Shq1 expression by western blotting (Figure 2). We found that Shq1 was expressed mainly at embryonic stages, with highest expression at E13.5-15.5, suggesting its important role in neurogenesis and/or neuronal migration.

To determine the functions of Shq1 during cortical neurogenesis and neuronal migration, we tested the effects of Shq1 loss-of-function on neural progenitors during

embryonic brain development. We used *in utero* electroporation of short-hairpin RNAs (shRNAs) to knock down Shq1 in the developing mouse cortex. To select the most efficient shRNA to knock down Shq1, three shRNA sequences targeting Shq1 3'UTR (shShq1#1) or coding region (shShq1#3 and shShq1#4) were inserted to pLKO_TRC005 vector, which also contains puromycin selection marker. These constructs were then each transfected to the mouse neuroblast cell line Neuro-2a (N2a). Cells were transfected for 24 hr followed by puromycin selection for 50 hr. Total RNAs were extracted from cells and mRNA level of Shq1 was detected by RT-qPCR. We found that Shq1 mRNA level in cells expressing 3 shRNAs were significantly lower compared to cells transfected with control shRNA (shCtrl) (Figure 3a).

We further examined Shq1 protein expression by western blotting. Cells were lysed after 24 hr of transfection followed by 50 hr of puromycin selection. We found that Shq1 protein expression in cells expressing all 3 shRNAs were slightly lower compared to cells transfected with shCtrl (Figure 3b, c).

We then electroporated shShq1 or shCtrl along with GFP in neural progenitors of developing mouse cortex at E14.5 using *in utero* electroporation. The distributions of GFP+ cells were observed in brain slices 4 day later at E18.5 (Figure 4a, c). We found that most GFP+ cells in the brains electroporated with shCtrl migrated to the CP (64.0 ± 7.7 %). In brains electroporated with shShq1#1, #3, and #4, most GFP+ cells were located in the IZ (shShq1#1: 40.9 ± 3.7 %; shShq1#3: 34.2 ± 3.4 %; shShq1#4: 29.4 ± 1.9 %; vs. shCtrl: 20.4 ± 4.3 %) and VZ/SVZ (shShq1#1: 45.5 ± 2.2 %; shShq1#3: 30.6 ± 3.1 %; shShq1#4: 35.1 ± 1.1 %; vs. shCtrl: 15.6 ± 4.2 %). Among all, shShq1#1 showed most severe effect on cell distribution, with only about 10% cells reaching the CP (13.7 ± 3.9 %). These results indicated that Shq1 loss-of-function altered cell distribution in the developing mouse cortex.

To avoid potential off-target effects of each Shq1 shRNA, we co-electroporated SHQ1 cDNA to rescue the effects of shShq1 in embryonic mouse brains. HA-tagged human SHQ1 cDNA was inserted to pCAGIG vector, which encoded IRES-GFP (pCAGIG-

SHQ1). We then electroporated pCAGIG-SHQ1 along with each shShq1 at E14.5. The distributions of GFP+ cells were observed in brain slices 4 days later at E18.5 (Figure 4a, b, c). In control brains electroporated with WT SHQ1 cDNA, most GFP+ cells migrated to the CP (62.2 ± 6.4 %), suggesting no detrimental effects in overexpressing SHQ1. In brains electroporated with WT SHQ1 cDNA along with shShq1#4, GFP+ cells located in SVZ were significantly decreased compared to brains electroporated with shShq1#4 (shShq1#4: 35.1 ± 1.1 % vs. WT+shShq1#4: 28.0 ± 1.5 %). Similarly, in brains electroporated with WT SHQ1 cDNA along with shShq1#1, GFP+ cells located in IZ significantly increased compared to brains electroporated with shShq1#1 (shShq1#1: 40.9 ± 3.7 % vs. WT+shShq1#1: 61.3 ± 1.2 %). However, WT SHQ1 cDNA was not able to rescue the migration defect in brains electroporated with shShq#3. These results suggested that migration delay caused by shShq1#1 and shShq1#4 could be partially rescued by expressing human SHQ1 in Shq1 knockdown cells.

3.2 Shq1 loss-of-function may not affect neural progenitor proliferation in developing mouse cortex

Since the patients carrying SHQ1 variants present microcephaly, we hypothesized that Shq1 loss-of-function may disrupt cell proliferation in the early stage of corticogenesis. Accordingly, we performed *in utero* electroporation of shShq1 at E14.5. The proliferation of GFP+ cells was observed in brain slices 2 day later at E16.5 by immunostaining of proliferation marker Ki67, which is expressed during G1, S, G2, and M phases of cell cycle. In control brains, about 30% of GFP+ cells were also Ki67+ (28.5 %), suggesting these cells were still in proliferation at this stage (Figure 5). Surprisingly, similar percentage of Ki67+ cells were found in brains electroporated with each Shq1 shRNA (shShq1#1: 19.5 ± 0.1 %; shShq1#3: 15.6 ± 3.0 %; shShq1#4: 29.5 ± 4.4 %; vs. shCtrl: 28.5 ± 3.3 %). This result suggested that Shq1 loss-of-function may not alter proliferation of neural progenitors.

3.3 Shq1 loss-of-function did not increase cell death in developing mouse cortex

Microcephaly could be caused by an decreased cell proliferation and/or increased cell death. Since we did not observe alteration in the number of proliferating neural progenitors in brains electroporated with shShq1, we speculated that Shq1 loss-of-function may induce cell death. Therefore, we examined cell death of GFP+ cells electroporated with shShq1 by *in utero* electroporation. The apoptosis of GFP+ cells were observed in brain slices at P28 by TUNEL staining, which labels DNA fragments in apoptotic cells. Brain slices treated with DNase I prior to TUNEL labeling were used as positive control. We found that there was nearly almost no TUNEL signal in brains electroporated with shCtrl or shShq1#1 (Figure 6). This result suggested that Shq1 loss-of-function did not increase apoptosis in neurons.

3.4 Shq1 knockdown cells could still differentiate into NeuN+ neurons

To examine whether these Shq1-knockdown cells were arrested at postnatal stages, we again performed *in utero* electroporation of shShq1 at E14.5 and examined the distributions of GFP+ cells in brain slices at P7. We found that most GFP+ cells (83.4 ± 2.1%) in the brains electroporated with shShq1#1 were arrested in white matter (WM). In brains electroporated with shCtrl, shShq1#3, and shShq1#4, most GFP+ cells (shCtrl: 95.4 ± 1.5 %; shShq1#3: 98.8 ± 1.2 %; shShq1#4: 96.5 ± 3.6 %) migrated to layer II/III of cortex (Ctx) (Figure 7a, b).

To examine whether Shq1 loss-of-function will affect neuronal differentiation, cell identity was observed at P7 by immunostaining of post-mitotic neuronal marker NeuN (RNA binding fox-1 homolog 3). Interestingly, in brains electroporated with shShq1 or shCtrl, nearly all cells were NeuN positive cells (Figure 7a, c). There was no significant difference between brains electroporated with Shq1 and control shRNAs (shShq1#1: 84.5 ± 6.8 %; shShq1#3: 84.8 ± 6.5 %; shShq1#4: 92.4 ± 3.9 %; vs. shCtrl: 89.9 ± 1.4

%). This result suggested that Shq1 loss-of-function had a minimal effect on neuronal differentiation.

3.5 Shq1 loss-of-function altered cortical projection without affecting cell fate

Although those Shq1 knockdown neurons could still differentiate into NeuN+ neurons, surprisingly, we found that the axonal projections of these GFP+ cells were altered in brains electroporated with shShq1#1. In brains electroporated with shCtrl, most GFP+ cells were callosal projection neurons, which extended axons across corpus callosum to contralateral hemisphere at P7, P14, and P21 (Figure 8a, c, e). However, in brains electroporated with shShq1#1, most GFP+ cells were arrested in the subcortical region and extended axons both across corpus callosum to contralateral hemisphere and laterally towards the ipsilateral external capsule (Figure 8b, d, f).

Since callosal projection neurons expressed Satb2 and subcortical projection neurons expressed Ctip2 (Hatanaka et al., 2015), we then surveyed the cell type of the GFP+ cells in brains electroporated with shShq1#1 and shCtrl by immunostaining of Satb2 and Ctip2. Surprisingly, similar to control brains, most GFP+ cells in brains electroporated with shShq1#1 were positive to Satb2 and negative to Ctip2 (Figure 9). These results suggested that Shq1 loss-of-function may alter cortical projections without affecting the fate of arrested cells in the developing mouse cortex.

3.6 SHQ1 variants failed to rescue the phenotypes caused by shShq1 in developing mouse cortex

Since the symptoms of SHQ1-related patients occurred only when both alleles of SHQ1 were mutated, we postulated that these SHQ1 variants may be loss-of-function mutations. Thus, we tested the ability of these variants in rescuing the migration defects

in the developing mouse cortex. First, we generated different SHQ1 variants by mutagenesis of the HA-tagged SHQ1 cDNAs. To test the expression of these plasmids, they were each transfected to human embryonic kidney cell line HEK293T for 24 hours. Cell lysates were harvested and the protein expression of SHQ1 were examined by western blotting. We found that L333V, R335C, and A426V variants were expressed in similar levels compared to WT SHQ1. Remarkably, Y65X expression almost disappeared in transfected cells (Figure 10a, b), potentially due to its very early termination in the peptide.

To test the ability of SHQ1 variants in rescuing neuronal migration defects by Shq1 knockdown, we next performed *in utero* electroporation of these SHQ1 variants along with shShq1 at E14.5. The distributions of GFP+ cells were observed 4 day later at E18.5. We found that in brains electroporated with Y65X along with shShq1, most GFP+ cells were remained in IZ (22.3 ± 5.1%) and SVZ (33.7 ± 9.2%; Figure 11a, b). The same results were observed in brains electroporated with L333V along with shShq1 (IZ: 21.9 ± 2.2%; SVZ: 34.4 ± 3.7%). These results indicated that SHQ1 variants failed to rescue abnormal neuronal cell distributions caused by shShq1.

3.7 SHQ1 variants attenuated their binding ability to DKC1 *in vitro*

SHQ1 is an essential assembly factor of H/ACA RNPs; when the biogenesis and function of H/ACA RNPs are disturbed, it would usually cause Dyskeratosis congenita. Therefore, to test whether our new SHQ1 mutations could disturb the biogenesis of H/ACA RNPs in neural progenitors, WT or mutant cDNAs were each transfected to HEK293T cells. Cells were lysed 24 hr later and the binding ability of different SHQ1 variants with H/ACA RNP core protein, DKC1, was examined by co-immunoprecipitation. We found that SHQ1 interaction to DKC1 was significantly reduced in cells expressing R335C and A426V variants compared to WT SHQ1 (Figure 12a, b), whereas there was no significant difference in L333V variant. This result indicated that most SHQ1 variants attenuated their binding ability to DKC1 which may disrupt the assembly and biogenesis of H/ACA RNPs.

Chapter 4: Discussion

In this study, we identified a patient with novel SHQ1 compound heterozygous variants, who suffered from developmental delay, movement disorder, and multiple neurological disorders. To investigate the pathogenic mechanisms of SHQ1 variants in brain development, we then modulated the expression of Shq1 in developing mouse cortex by in utero electroporation of Shq1 shRNAs. We found that loss of Shq1 caused multiple disorders in cerebral cortex development including delay of radial neuronal migration, and alteration of cortical projection, which could be associated with clinical features of SHQ1-related patients.

4.1 Potential roles of SHQ1 in neuronal migration

Disturbance of radial neuronal migration can cause several cortical malformations. Some would affect the appearance of brain surface, such as lissencephaly and cobblestone complex, while some would have mislocalized mature neurons with no lamination defects, such as heterotopia.

In our results, we observed radial neuronal migration delay in Shq1 knockdown brains 4 days after *in utero* electroporation until P28 (Figure 4). These delayed cells could still differentiate into NeuN+ neurons (Figure 7). However, our patient with SHQ1 compound heterozygous mutations does not have smooth brain surface. Therefore, in-depth examination of brain MRI of our patient need to be performed in order to track down evidences related to neuronal migration delay. We predicted that SHQ1 loss-of-function may be related to heterotopia, because heterotopia is a group of mature neurons resided in white matter, which correlates with our observation in brains electroporated with shShq1.

4.2 Potential roles of SHQ1 in callosal projection

The projections of callosal projection neurons (CPN) vary greatly in the directions of axon extension and the axonal targets of brain area. Subpopulations of CPNs extend their axons both contralaterally across corpus callosum and ipsilaterally toward striatum, premotor cortex, or sensorimotor cortex (Cauller *et al.*, 1998; Mitchell and Macklis, 2005; Wilson, 1987). Dual projections of CPNs begin to appear at postnatal day 8 in mice and are refined at about postnatal day 21 (Mitchell and Macklis, 2005).

Here, we observed dual projections in shShq1 electroporated cells at P7, P14, and P21. These cells extended their axons through corpus collosum to contralateral cortex and also projected their axons towards ipsilateral claustrum (Figure 8). Although evidences have been found that some deep layer CPNs would extend their axons to claustrum (Veinante and Deschênes, 2003). The molecular controls of this kind of projection are poorly understood.

Another possibility is that SHQ1 loss-of-function may affect other transcription factors related to axon projection. For instance, neurogenin 2 (Ngn2) was found to regulate callosal projection. Loss of Ngn2 could cause the axon of layer II/III cortical neurons project laterally toward abnormal brain area (Hand and Polleux, 2011). Therefore, to investigate the potential causes of abnormal axon projection in Shq1 KD brains, RNA-seq will be used to select downstream targets.

4.3 Potential roles of SHQ1 in microcephaly and cerebellar atrophy

H/ACA RNPs play important roles in mRNA splicing. SHQ1 particularly has been reported to be essential for the cell survival of T-acute lymphoblastic leukemia (T-ALL), which is a severe form of blood cancer. SHQ1 depletion can affect pre-mRNA splicing in many genes, especially MYC, which regulates cell proliferation, differentiation, and

apoptosis, etc (Su et al., 2018).

However, according to immunostaining of Ki67 and TUNEL assay in brains electroporated with Shq1 shRNAs, we did not observe decreased neural progenitor proliferation and increased neuronal apoptosis, which are the signs of microcephaly (Figure 5, 6). Even so, it needs to be noted that TUNEL assay labels DNA fragments of apoptotic cells, which represents the relatively late stages of apoptosis compared to caspase activation and cytochrome c release. Therefore, we should further use different methods, such as western blot of pro- and active caspase, to check whether GFP+ cells in brains electroporated with Shq1 shRNAs are undergoing programmed cell death at P28 or older age.

Since SHQ1 is crucial for mRNA splicing, we assume that loss of SHQ1 may impair mRNA splicing of gene related to microcephaly, namely CENPJ (centromere protein J), CEP152 (centrosomal protein 152), and CDK6 (cyclin-dependent kinase 6) etc. Accordingly, RNA-Seq and minigene assay will be used to select downstream targets upon SHQ1 loss-of-function.

It needs to be noted that patients with SHQ1 compound heterozygous mutations also suffer from cerebellar atrophy. Therefore, to link the phenotypes of patients with SHQ1 mutations with that of Shq1 KD mouse, in vivo electroporation of Shq1 shRNAs in granule progenitors of mouse cerebellum at P6 will be performed. The proliferation of electroporated cells will be observed in brain slices 1.5 day after.by immunostaining of Ki67.

4.4 Potential pathogenic mechanisms of SHQ1 variants

SHQ1, an assembly factor, are vital for the biogenesis of H/ACA RNPs. SHQ1 can function as an RNA mimic to preclude unspecific RNA from binding to H/ACA RNP

complex (Walbott et al., 2011). When SHQ1 is knockdown or mutated in mammalian cells and yeast, it would disrupt the accumulation of H/ACA RNAs (Grozdanov et al., 2009; Singh et al., 2009; Sleiman *et al.*, 2022).

Based on our co-immunoprecipitation results, we found that two reported variants, R335C and A426V, attenuated their binding ability to DKC1 (Figure 12). However, the protein expression of Y65X, one of our patient variants, was almost absent in transfected cells (Figure 10). Another variant in our patient, L333V, did not affect its binding to DKC1. Therefore, we propose two possibilities: (1) by affecting the structure of DKC1; (2) by affecting mechanisms outside of H/ACA RNPs pathway.

DKC1 is first synthesized in cytoplasm. Since DKC1 is unstable on its own, it is hypothesized that SHQ1 would bind with DKC1 to protect from aggregation and degradation (Singh *et al.*, 2009). However, it is largely unknown what is the exact effects of the formation of SHQ1-DKC1 complex. Thus, we propose that although L333V variants can bind with DKC1, L333V variants may to some extent influence the structure of DKC1, and as a result, disturb the biogenesis of H/ACA RNPs. To test this hypothesis, we will examine the expression of H/ACA RNAs in cells transfected with SHQ1 variants by RT-qPCR.

In addition to the biogenesis of H/ACA RNPs, SHQ1 had also been reported to participate in other mechanisms. For instance, SHQ1 would respond to ER stress and promote tumor apoptosis in hepatocellular carcinoma cells (Liu et al., 2020). SHQ1 were also found to be deleted in prostate cancer, suggesting its role in inhibiting prostate cancer growth (Hieronymus et al., 2017). However, little is known about the role of SHQ1 in neurons and brain development. Therefore, the downstream targets of SHQ1 in brain development are worth exploring in order to provide potential pathogenic mechanisms in SHQ1-related disorders.

Chapter 5: Reference

Alcamo, E.A., Chirivella, L., Dautzenberg, M., Dobreva, G., Fariñas, I., Grosschedl, R., and McConnell, S.K. (2008). Satb2 regulates callosal projection neuron identity in the developing cerebral cortex. Neuron *57*, 364-377. 10.1016/j.neuron.2007.12.012.

AlSabbagh, M.M. (2020). Dyskeratosis congenita: a literature review. J Dtsch Dermatol Ges *18*, 943-967. 10.1111/ddg.14268.

Arlotta, P., Molyneaux, B.J., Chen, J., Inoue, J., Kominami, R., and Macklis, J.D. (2005). Neuronal subtype-specific genes that control corticospinal motor neuron development in vivo. Neuron *45*, 207-221. 10.1016/j.neuron.2004.12.036.

Balakin, A.G., Smith, L., and Fournier, M.J. (1996). The RNA world of the nucleolus: two major families of small RNAs defined by different box elements with related functions. Cell *86*, 823-834. 10.1016/s0092-8674(00)80156-7.

Barkovich, A.J., Kuzniecky, R.I., Dobyns, W.B., Jackson, G.D., Becker, L.E., and Evrard, P. (1996). A classification scheme for malformations of cortical development. Neuropediatrics *27*, 59-63. 10.1055/s-2007-973750.

Barkovich, A.J., Kuzniecky, R.I., Jackson, G.D., Guerrini, R., and Dobyns, W.B. (2001). Classification system for malformations of cortical development: update 2001. Neurology *57*, 2168-2178. 10.1212/wnl.57.12.2168.

Battaglia, G., Granata, T., Farina, L., D'Incerti, L., Franceschetti, S., and Avanzini, G. (1997). Periventricular nodular heterotopia: epileptogenic findings. Epilepsia *38*, 1173-1182. 10.1111/j.1528-1157.1997.tb01213.x.

Bizarro, J., and Meier, U.T. (2017). Inherited SHQ1 mutations impair interaction with NAP57/dyskerin, a major target in dyskeratosis congenita. Mol Genet Genomic Med *5*, 805-808. 10.1002/mgg3.314.

Britanova, O., de Juan Romero, C., Cheung, A., Kwan, K.Y., Schwark, M., Gyorgy, A., Vogel, T., Akopov, S., Mitkovski, M., Agoston, D., et al. (2008). Satb2 is a postmitotic determinant for upper-layer neuron specification in the neocortex. Neuron *57*, 378-392. 10.1016/j.neuron.2007.12.028.

Cauller, L.J., Clancy, B., and Connors, B.W. (1998). Backward cortical projections to primary somatosensory cortex in rats extend long horizontal axons in layer I. J Comp Neurol *390*, 297-310.

Cohn, W.E. (1960). Pseudouridine, a Carbon-Carbon Linked Ribonucleoside in Ribonucleic Acids: Isolation, Structure, and Chemical Characteristics. Journal of Biological Chemistry *235*, 1488-1498. https://doi.org/10.1016/S0021-9258(18)69432-3.

Cohn, W.E., and Volkin, E. (1951). Nucleoside-5′-Phosphates from Ribonucleic Acid. Nature *167*, 483-484. 10.1038/167483a0.

Darzacq, X., Jády, B.E., Verheggen, C., Kiss, A.M., Bertrand, E., and Kiss, T. (2002). Cajal body-specific small nuclear RNAs: a novel class of 2'-O-methylation and pseudouridylation guide RNAs. EMBO J *21*, 2746-2756. 10.1093/emboj/21.11.2746.

Davis, F.F., and Allen, F.W. (1957). RIBONUCLEIC ACIDS FROM YEAST WHICH CONTAIN A FIFTH NUCLEOTIDE. Journal of Biological Chemistry *227*, 907-915. https://doi.org/10.1016/S0021-9258(18)70770-9.

des Portes, V., Pinard, J.M., Billuart, P., Vinet, M.C., Koulakoff, A., Carrié, A., Gelot, A., Dupuis, E., Motte, J., Berwald-Netter, Y., et al. (1998). A novel CNS gene required for neuronal migration and involved in X-linked subcortical laminar heterotopia and lissencephaly syndrome. Cell *92*, 51-61. 10.1016/s0092-8674(00)80898-3.

Dobyns, W.B., Kirkpatrick, J.B., Hittner, H.M., Roberts, R.M., and Kretzer, F.L. (1985). Syndromes with lissencephaly. II: Walker-Warburg and cerebro-oculo-muscular syndromes and a new syndrome with type II lissencephaly. Am J Med Genet *22*, 157-195. 10.1002/ajmg.1320220118.

Dobyns, W.B., Reiner, O., Carrozzo, R., and Ledbetter, D.H. (1993). Lissencephaly. A human brain malformation associated with deletion of the LIS1 gene located at chromosome 17p13. Jama *270*, 2838-2842. 10.1001/jama.270.23.2838.

Dubeau, F., Tampieri, D., Lee, N., Andermann, E., Carpenter, S., Leblanc, R., Olivier, A., Radtke, R., Villemure, J.G., and Andermann, F. (1995). Periventricular and subcortical nodular heterotopia. A study of 33 patients. Brain *118 (Pt 5)*, 1273-1287. 10.1093/brain/118.5.1273.

Ganot, P., Caizergues-Ferrer, M., and Kiss, T. (1997). The family of box ACA small nucleolar RNAs is defined by an evolutionarily conserved secondary structure and ubiquitous sequence elements essential for RNA accumulation. Genes Dev *11*, 941-956. 10.1101/gad.11.7.941.

Gleeson, J.G., Allen, K.M., Fox, J.W., Lamperti, E.D., Berkovic, S., Scheffer, I., Cooper, E.C., Dobyns, W.B., Minnerath, S.R., Ross, M.E., and Walsh, C.A. (1998). Doublecortin, a brain-specific gene mutated in human X-linked lissencephaly and double cortex syndrome, encodes a putative signaling protein. Cell *92*, 63-72. 10.1016/s0092-8674(00)80899-5.

Grozdanov, P.N., Roy, S., Kittur, N., and Meier, U.T. (2009). SHQ1 is required prior to NAF1 for assembly of H/ACA small nucleolar and telomerase RNPs. RNA *15*, 1188-1197. 10.1261/rna.1532109.

Hand, R., and Polleux, F. (2011). Neurogenin2 regulates the initial axon guidance of cortical pyramidal neurons projecting medially to the corpus callosum. Neural Dev *6*, 30. 10.1186/1749-8104-6-30.

Hatanaka, Y., Namikawa, T., Yamauchi, K., and Kawaguchi, Y. (2015). Cortical Divergent Projections in Mice Originate from Two Sequentially Generated, Distinct Populations of Excitatory Cortical Neurons with Different Initial Axonal Outgrowth Characteristics. Cerebral Cortex *26*, 2257-2270. 10.1093/cercor/bhv077.

Haubensak, W., Attardo, A., Denk, W., and Huttner, W.B. (2004). Neurons arise in the basal neuroepithelium of the early mammalian telencephalon: a major site of neurogenesis. Proc Natl Acad Sci U S A *101*, 3196-3201. 10.1073/pnas.0308600100.

Hieronymus, H., Iaquinta, P.J., Wongvipat, J., Gopalan, A., Murali, R., Mao, N., Carver, B.S., and Sawyers, C.L. (2017). Deletion of 3p13-14 locus spanning FOXP1 to SHQ1 cooperates with PTEN loss in prostate oncogenesis. Nat Commun *8*, 1081. 10.1038/s41467-017-01198-9.

Hoyeraal, H.M., Lamvik, J., and Moe, P.J. (1970). Congenital hypoplastic thrombocytopenia and cerebral malformations in two brothers. Acta Paediatr Scand *59*, 185-191. 10.1111/j.1651-2227.1970.tb08986.x.

Hreidarsson, S., Kristjansson, K., Johannesson, G., and Johannsson, J.H. (1988). A syndrome of progressive pancytopenia with microcephaly, cerebellar hypoplasia and growth failure. Acta Paediatr Scand *77*, 773-775. 10.1111/j.1651-2227.1988.tb10751.x.

Lafontaine, D.L., Bousquet-Antonelli, C., Henry, Y., Caizergues-Ferrer, M., and Tollervey, D. (1998). The box H + ACA snoRNAs carry Cbf5p, the putative rRNA pseudouridine synthase. Genes Dev *12*, 527-537. 10.1101/gad.12.4.527.

Leviton, A., Holmes, L.B., Allred, E.N., and Vargas, J. (2002). Methodologic issues in epidemiologic studies of congenital microcephaly. Early Human Development *69*, 91-105. https://doi.org/10.1016/S0378-3782(02)00065-8.

Liu, H., Xie, S., Fang, F., Kalvakolanu, D.V., and Xiao, W. (2020). SHQ1 is an ER stress response gene that facilitates chemotherapeutics-induced apoptosis via sensitizing ER-stress response. Cell Death Dis *11*, 445. 10.1038/s41419-020-2656-0.

Mitchell, B.D., and Macklis, J.D. (2005). Large-scale maintenance of dual projections by callosal and frontal cortical projection neurons in adult mice. J Comp Neurol *482*, 17-32. 10.1002/cne.20428.

Mitchell, J.R., Cheng, J., and Collins, K. (1999). A box H/ACA small nucleolar RNA-like domain at the human telomerase RNA 3' end. Mol Cell Biol *19*, 567-576. 10.1128/mcb.19.1.567.

Nadarajah, B., Brunstrom, J.E., Grutzendler, J., Wong, R.O.L., and Pearlman, A.L. (2001). Two modes of radial migration in early development of the cerebral cortex. Nature Neuroscience *4*, 143-150. 10.1038/83967.

Noctor, S.C., Flint, A.C., Weissman, T.A., Dammerman, R.S., and Kriegstein, A.R. (2001). Neurons derived from radial glial cells establish radial units in neocortex. Nature *409*, 714-720. 10.1038/35055553.

Noctor, S.C., Flint, A.C., Weissman, T.A., Wong, W.S., Clinton, B.K., and Kriegstein, A.R. (2002). Dividing Precursor Cells of the Embryonic Cortical Ventricular Zone Have Morphological and Molecular Characteristics of Radial Glia. The Journal of Neuroscience *22*, 3161. 10.1523/JNEUROSCI.22-08-03161.2002.

Noctor, S.C., Martínez-Cerdeño, V., Ivic, L., and Kriegstein, A.R. (2004). Cortical neurons arise in symmetric and asymmetric division zones and migrate through specific phases. Nat Neurosci *7*, 136-144. 10.1038/nn1172.

O'Leary, D.D., and Koester, S.E. (1993). Development of projection neuron types, axon pathways, and patterned connections of the mammalian cortex. Neuron *10*, 991-1006. 10.1016/0896-6273(93)90049-w.

Rakic, P. (1972). Mode of cell migration to the superficial layers of fetal monkey neocortex. J Comp Neurol *145*, 61-83. 10.1002/cne.901450105.

Rakic, P. (1974). Neurons in rhesus monkey visual cortex: systematic relation between time of origin and eventual disposition. Science *183*, 425-427. 10.1126/science.183.4123.425.

Raymond, A.A., Fish, D.R., Stevens, J.M., Sisodiya, S.M., Alsanjari, N., and Shorvon, S.D. (1994). Subependymal heterotopia: a distinct neuronal migration disorder associated with epilepsy. J Neurol Neurosurg Psychiatry *57*, 1195-1202. 10.1136/jnnp.57.10.1195.

Schell-Apacik, C.C., Wagner, K., Bihler, M., Ertl-Wagner, B., Heinrich, U., Klopocki, E., Kalscheuer, V.M., Muenke, M., and von Voss, H. (2008). Agenesis and dysgenesis of the corpus callosum: clinical, genetic and neuroimaging findings in a series of 41 patients. Am J Med Genet A *146a*, 2501-2511. 10.1002/ajmg.a.32476.

Singh, M., Gonzales, F.A., Cascio, D., Heckmann, N., Chanfreau, G., and Feigon, J. (2009). Structure and functional studies of the CS domain of the essential H/ACA ribonucleoparticle assembly protein SHQ1. J Biol Chem *284*, 1906-1916. 10.1074/jbc.M807337200.

Sleiman, S., Marshall, A.E., Dong, X., Mhanni, A., Alidou-D'Anjou, I., Frosk, P., Marin, S.E., Stark, Z., Del Bigio, M.R., McBride, A., et al. (2022). Compound heterozygous variants in SHQ1 are associated with a spectrum of neurological features, including early-onset dystonia. Hum Mol Genet *31*, 614-624. 10.1093/hmg/ddab247.

Su, H., Hu, J., Huang, L., Yang, Y., Thenoz, M., Kuchmiy, A., Hu, Y., Li, P., Feng, H., Zhou, Y., et al. (2018). SHQ1 regulation of RNA splicing is required for T-

lymphoblastic leukemia cell survival. Nature Communications *9*, 4281. 10.1038/s41467-018-06523-4.

Tabata, H., and Nakajima, K. (2003). Multipolar Migration: The Third Mode of Radial Neuronal Migration in the Developing Cerebral Cortex. The Journal of Neuroscience *23*, 9996. 10.1523/JNEUROSCI.23-31-09996.2003.

Taylor, M., and David, A.S. (1998). Agenesis of the corpus callosum: a United Kingdom series of 56 cases. J Neurol Neurosurg Psychiatry *64*, 131-134. 10.1136/jnnp.64.1.131.

Veinante, P., and Deschênes, M. (2003). Single-cell study of motor cortex projections to the barrel field in rats. J Comp Neurol *464*, 98-103. 10.1002/cne.10769.

Walbott, H., Machado-Pinilla, R., Liger, D., Blaud, M., Réty, S., Grozdanov, P.N., Godin, K., van Tilbeurgh, H., Varani, G., Meier, U.T., and Leulliot, N. (2011). The H/ACA RNP assembly factor SHQ1 functions as an RNA mimic. Genes Dev *25*, 2398-2408. 10.1101/gad.176834.111.

Wilson, C.J. (1987). Morphology and synaptic connections of crossed corticostriatal neurons in the rat. J Comp Neurol *263*, 567-580. 10.1002/cne.902630408.

Yang, P.K., Rotondo, G., Porras, T., Legrain, P., and Chanfreau, G. (2002). The Shq1p.Naf1p complex is required for box H/ACA small nucleolar ribonucleoprotein particle biogenesis. J Biol Chem *277*, 45235-45242. 10.1074/jbc.M207669200.

Zinsser, F. (1906) Atropha cutis reticularis cum pigmentatione, dystrophia ungiumet leukoplakia oris. Ikonogr Dermatol (Hyoto), 5, 219 223.

Engman, M.F. (1926) A unique case of reticular pigmentation of the skin with atrophy. Archives of Dermatology and Syphiligraphie, 13, 685 687.

Moore, K. L., Persaud, T. V. N., & Torchia, M. G. (2016). The developing human: Clinically oriented embryology (10th ed.). Philadelphia, PA: Elsevier.

Sadler, T. W., & Langman, J. (2012). Langman's medical embryology (12th ed.). Philadelphia: Wolters Kluwer Health/Lippincott Williams & Wilkins.

Table 1.

	This study	Bizarro and Meier et al.	Sleiman et al.			
SHQ1 variants	p.Leu333Val (c.997C>G)/ p.Tyr65Ter (c.195T>A)	p.Arg335Cys (c.1003C>T)/ p.Ala426Val (c.1277C>T)	p.Glu292Lys (c.874G > A) / p.Asp277SerfsTer27 (c.828_831del)		p.Asp175Tyr (c.523G > T) / p.Asp277SerfsTer27 (c.828_831del)	
Developmental delay	Yes	Yes	Yes	Yes	No	No
Movement disorders	Dystonia, Orofacial dyskinesia, Truncal, extremities dyskinesia	Spastic quadriplegia	Dystonia, Hypotonia (Central and appendicular)	Dystonia, Hypotonia (Central and appendicular)	Dystonia	Dystonia
Epilepsy	Yes, well controlled under anti-epileptic medications	Yes, Intractable epilepsy	Yes, died of SUDEP	Yes, controlled with monotherapy	No	No
Brain MRI	Microcephaly, Cerebellar atrophy	Cerebellar hypoplasia, Microcephaly	Subtle cerebellar atrophy	Normal	Normal	Normal
Current state	Wheel-chair bound	Vegetative state	Died at age 10	N.d.	N.d.	N.d.

Figure 1

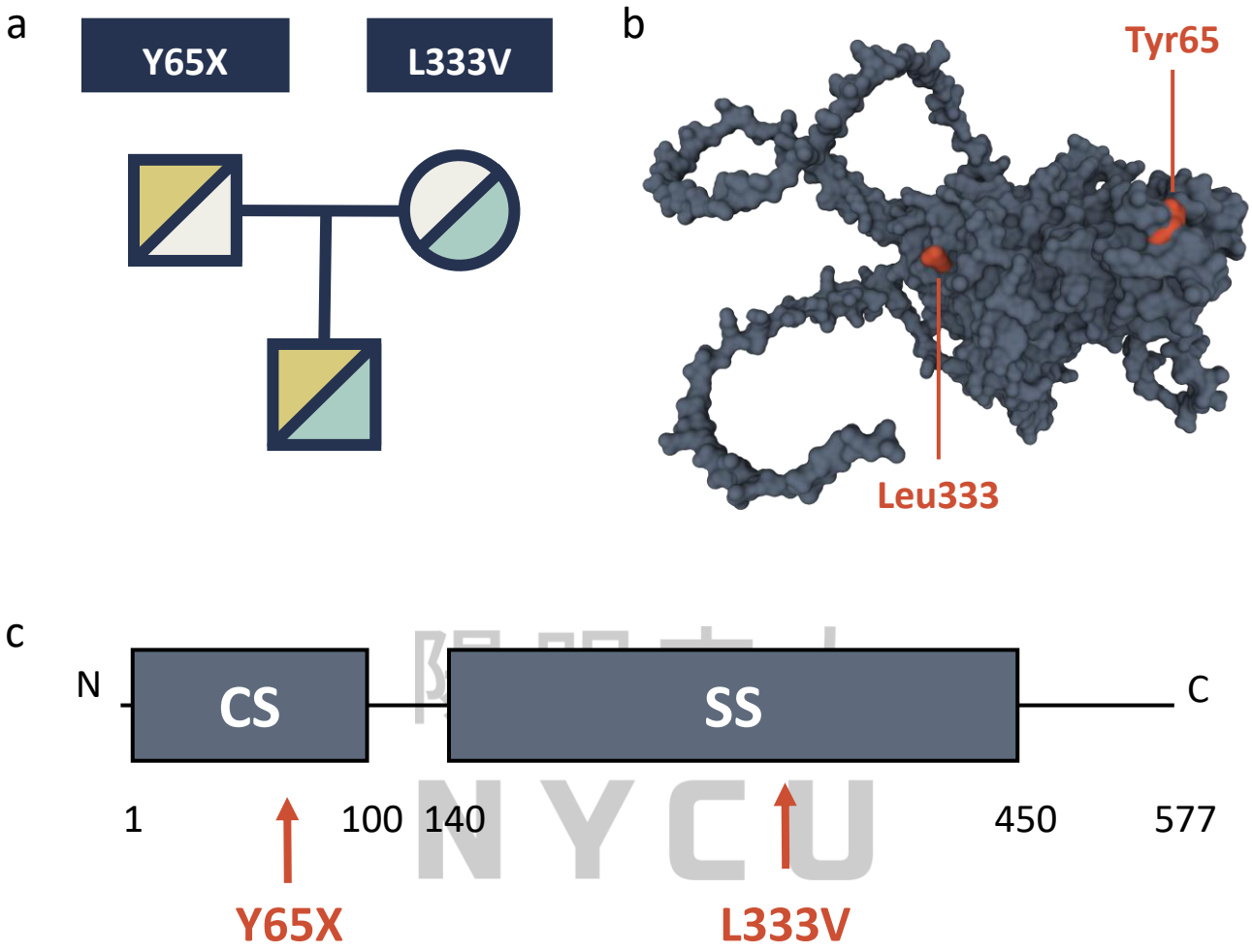

Figure 1. Pedigree of novel SHQ1 mutations and location of reported SHQ1 mutations. (a) Schematic of SHQ1 compound heterozygous mutations identified from patient. Novel variants p.Leu333Val (c.997C>G) and p.Tyr65Ter (c.195T>A) were inherited from father and mother respectively. (b) Predicted protein structure of human SHQ1 with novel variant sites. The novel SHQ1 variant sites were showed in red. (c) The protein domains of SHQ1 which consist of CS (CHORD-containing proteins and SGT1) and SS (SHQ1-specific) domains. The red arrows represented the novel variant sites of SHQ1.

Figure 2

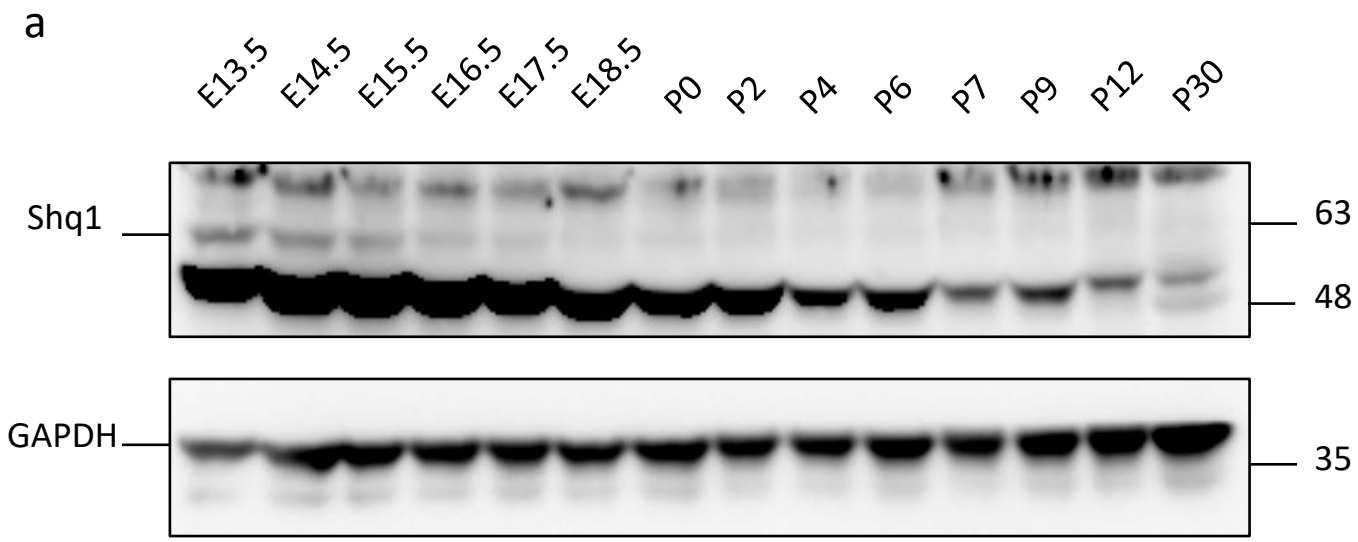

Figure 2. Shq1 was expressed in the developing mouse cortex. (a) Western blot of Shq1 expression in embryonic mouse cortex lysates (E13.5, E14.5, E15.5, E16.5, E17.5, E18.5) and in postnatal mouse cortex lysates (P0, P2, P4, P6, P7, P9, P12, P30). GAPDH was used as loading control.

Figure 3

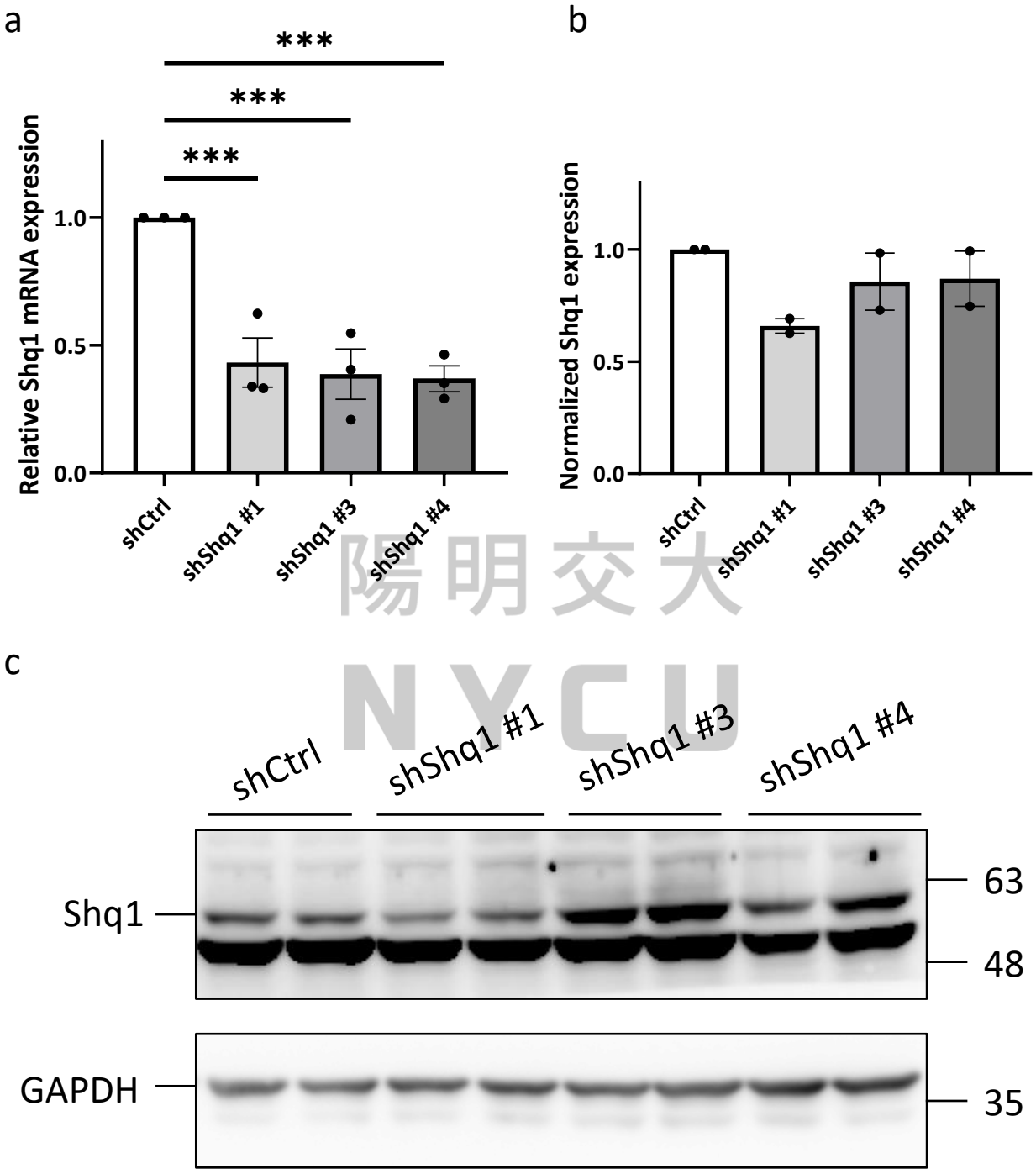

Figure 3. Both mRNA and protein level of Shq1 could be knockdown by shRNAs. (a) Bar plot of relative Shq1 mRNA level in N2a cells transfected with control and Shq1 shRNAs detected by RT-qPCR. N=3 in each group. Relative Shq1 mRNA levels were

significantly lower in cells transfected with shShq1 compared to shCtrl. Error bar represented SEM. Ordinary one-way ANOVA tests. *p<0.05, **p<0.01, ***p<0.001 (b) Bar plot of normalized Shq1 protein level in N2a cells transfected with control and Shq1 shRNAs. N=2 in all groups. Error bar represented SEM. Ordinary one-way ANOVA tests. (c) Western blot of Shq1 expression in N2a cells transfected with control and Shq1 shRNAs. GAPDH was used as loading control. Shq1 protein expression in cells transfected with shShq1 was slightly lower than in cells transfected with shCtrl.

Figure 4

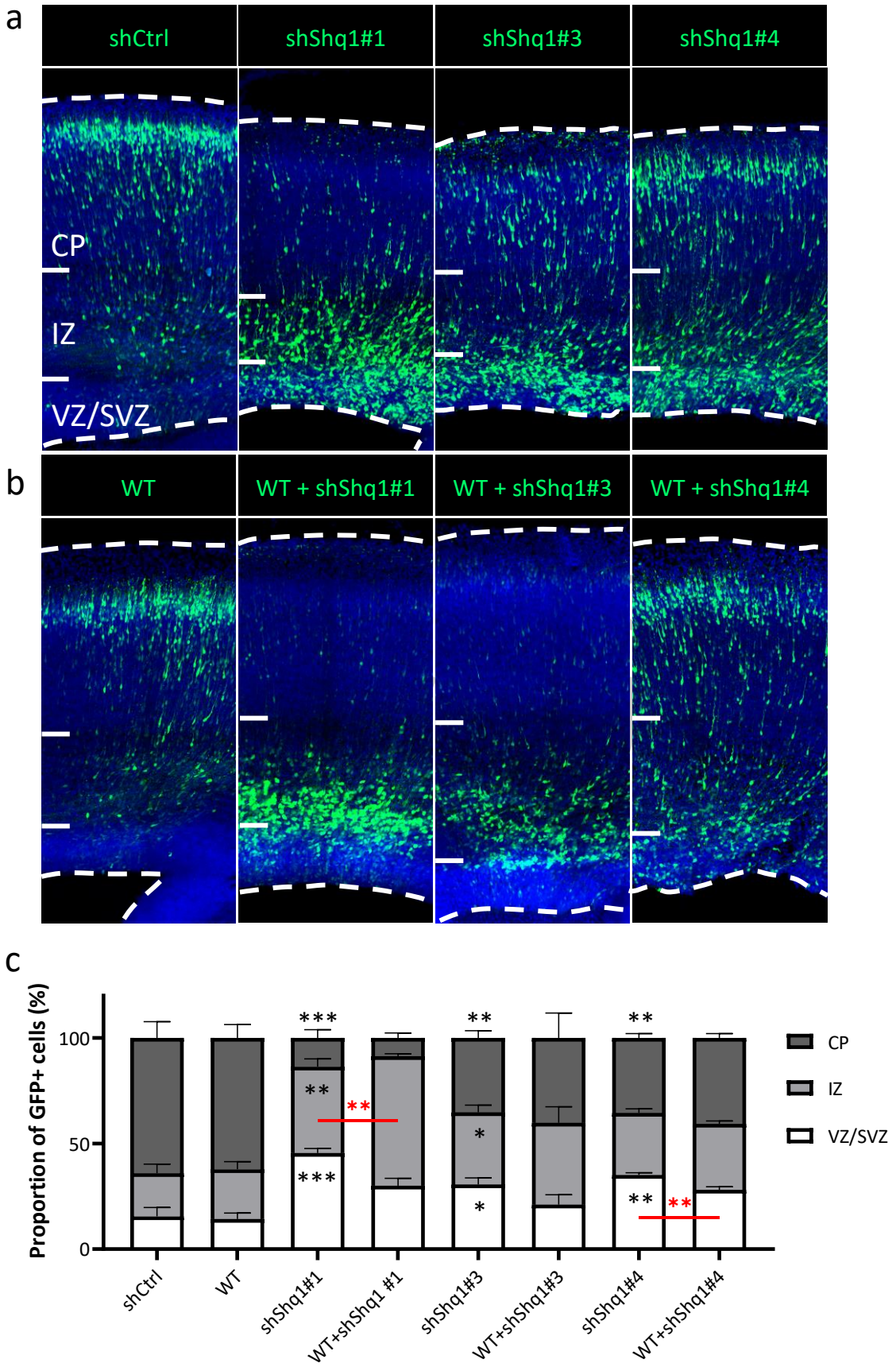
a
shCtrl
shShq1#1
shShq1#3
shShq1#4
CP
IZ
VZ/SVZ
b
WT
WT + shShq1#1
WT + shShq1#3
WT + shShq1#4
c
Proportion of GFP+ cells (%)
100
50
0
CP
IZ
VZ/SVZ
shCtrl
WT
shShq1#1
WT+shShq1 #1
shShq1#3
WT+shShq1#3
shShq1#4
WT+shShq1#4

Figure 4. Shq1 loss-of-function delayed neuronal migration in neural progenitors of developing mouse cortex. (a) Cell distributions of brains electroporated with shCtrl or shShq1 (shShq1#1, #3, and #4) at E18.5. Most GFP+ cells (green) in brains electroporated with shCtrl migrated to CP. However, in brains electroporated with shShq1, most GFP+ cells were delayed in SVZ/VZ and IZ. DAPI (blue) was used for nucleic acid staining. (b) Cell distributions of brains electroporated with SHQ1 WT cDNA or WT cDNA along with shShq1 at E18.5. More GFP+ cells migrated to IZ in brains electroporated with WT cDNA and shShq1#1 compared to shShq1#1 only. In brains electroporated with WT cDNA along with shShq1#4, GFP+ cells located in SVZ significantly decreased compared to brains electroporated with shShq1#4 only. DAPI (blue) was used for nucleic acid staining. (c) Bar plot of cell distributions in brains electroporated with shCtrl, shShq1, WT cDNA, or WT cDNA along with shShq1. shCtrl: N=7 mice; WT: N=2 mice; shShq1#1: N=5 mice; WT+shShq1#1: N=2 mice; shShq1#3: N=6 mice; WT+shShq1#3: N=3 mice; shShq1#4: N=6 mice; WT+shShq1#4: N=5 mice. Error bar represented SEM. Brown-Forsythe and Welch ANOVA tests. Black asterisks compared the marked bars to shCtrl. Red asterisks compared the two indicated bars. *p<0.05, **p<0.01, ***p<0.001

Figure 5

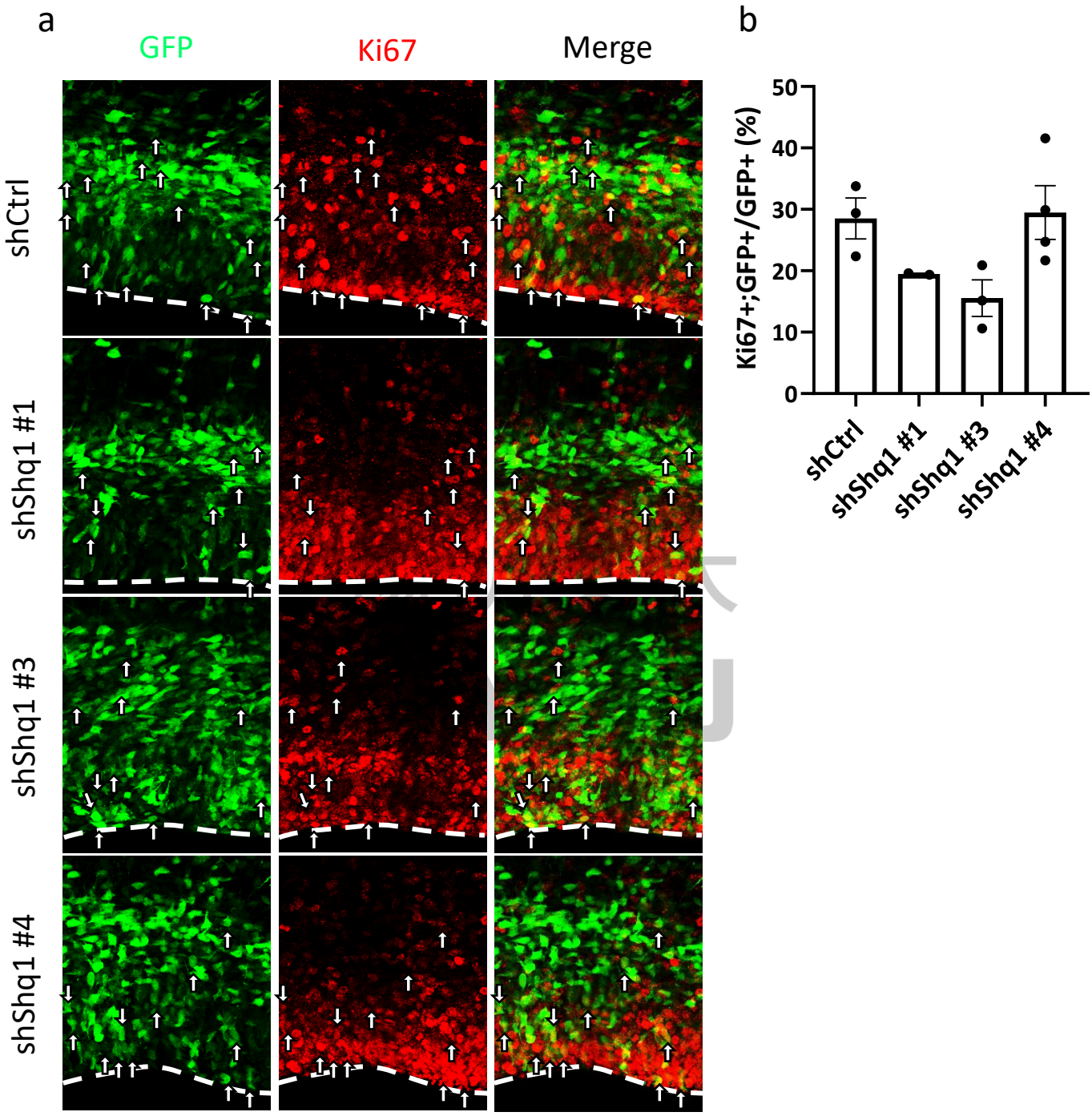

Figure 5. Shq1 KD may not affect cell proliferation in developing mouse cortex. (a) Immunostaining of Ki67 (red) in brains electroporated with shCtrl and shShq1 at E16.5. The percentages of Ki67+ cells in brains electroporated with shShq1 were similar in control brains. White arrows represented the colocalization of Ki67 and GFP signal.

(b) Bar plot of the percentage of Ki67+ cells in brains electroporated with control or Shq1 shRNAs. shCtrl: N=3 mice; shShq1#1: N=2 mice; shShq1#3: N=3 mice; shShq1#4: N=4 mice. Error bar represented SEM. Brown-Forsythe and Welch ANOVA tests.

Figure 6

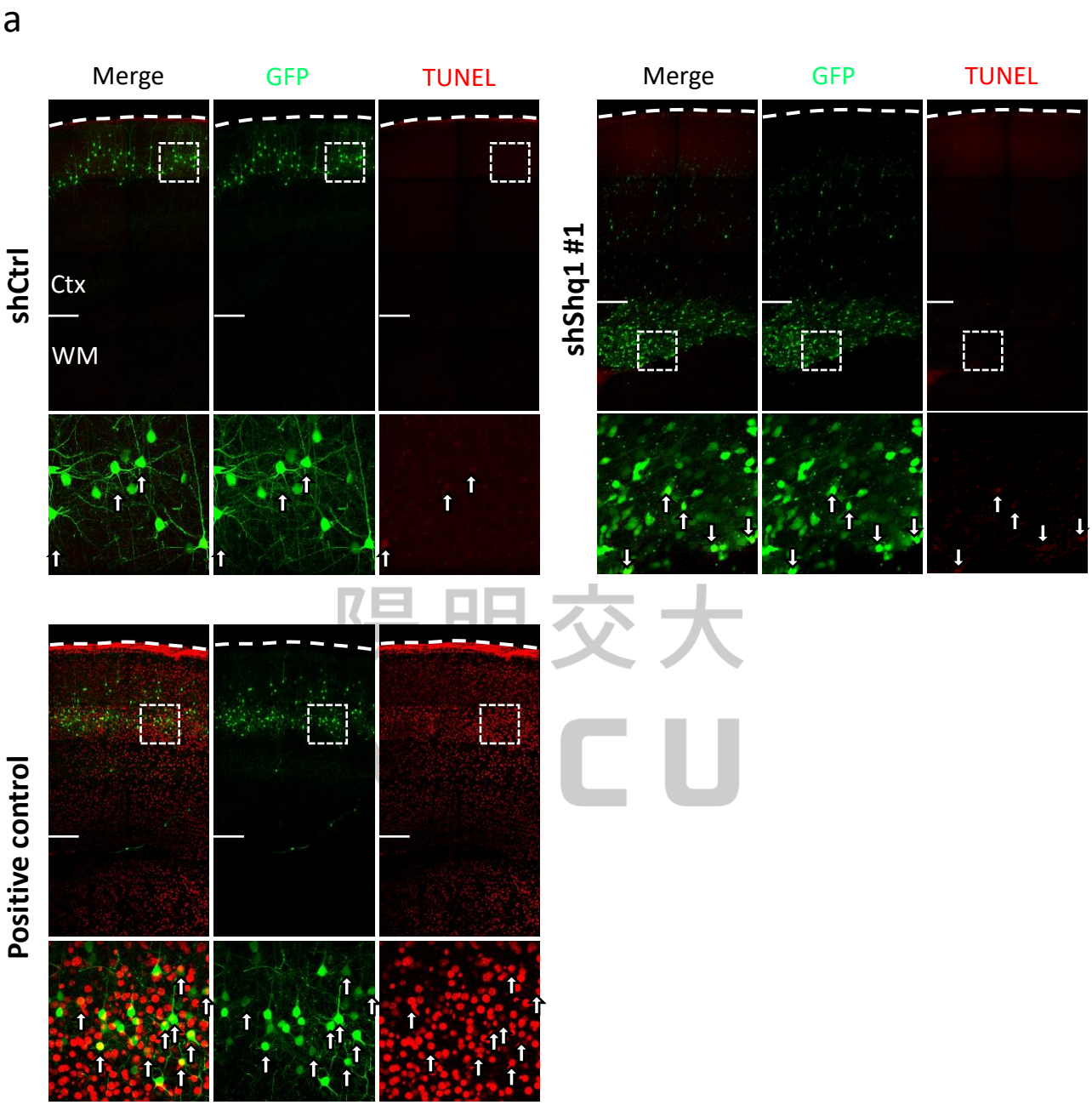

Figure 6. Loss of Shq1 may not induce neuronal apoptosis. (a) TUNEL staining of brains electroporated with shCtrl or shShq1#1. There were almost no TUNEL signal in brains electroporated with control and Shq1 shRNA. DNase I-treated brain slices, which induced DNA strand breaks, were used as positive control. White arrows represented the colocalization of TUNEL (red) and GFP (green) signal, which indicated apoptotic GFP+ cells.

Figure 7

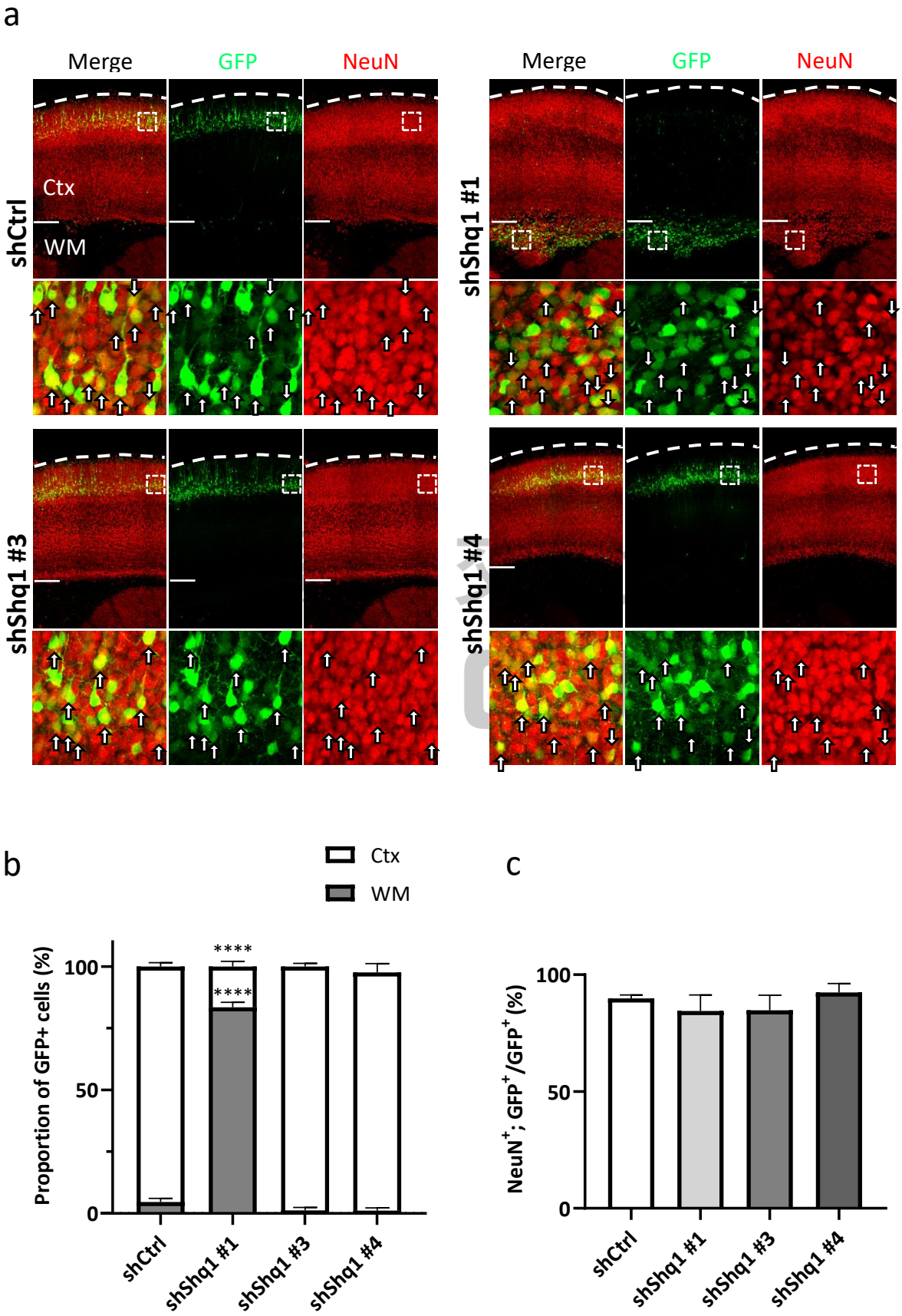
a
Merge
GFP
NeuN
shCtrl
Ctx
WM
shShq1 #1
shShq1 #3
shShq1 #4
b
Ctx
WM
Proportion of GFP+ cells (%)
100
50
0
****
****
shCtrl
shShq1 #1
shShq1 #3
shShq1 #4
c
NeuN+; GFP+/GFP+ (%)
100
50
0
shCtrl
shShq1 #1
shShq1 #3
shShq1 #4

Figure 7. Shq1 KD cells could differentiate to NeuN+ cells. (a) Immunostaining of NeuN (red) in brains electroporated with shCtrl and shShq1 at P7. In brains electroporated with shCtrl, shShq1#3, and shShq1#4, nearly all GFP+ cells migrated to layer II/III of the cortex. However, in brains electroporated with shShq1#1, most GFP+ cells were arrested in WM. Furthermore, the majority of GFP+ cells was NeuN+ in both control and KD brains. White arrows represented the colocalization of NeuN and GFP signal. (b) Bar plot of cell distribution in brains electroporated with control and Shq1 shRNAs. shCtrl: N=3 mice; shShq1#1: N=3 mice; shShq1#3: N=3 mice; shShq1#4: N=2 mice. Error bar represented SEM. Brown-Forsythe and Welch ANOVA tests. ****$p<0.0001$ (c) Bar plot of the percentage of Ki67+ cells in brains electroporated with control or Shq1 shRNAs. shCtrl: N=3 mice; shShq1#1: N=3 mice; shShq1#3: N=3 mice; shShq1#4: N=2 mice. Error bar represented SEM. Brown-Forsythe and Welch ANOVA tests.

Figure 8

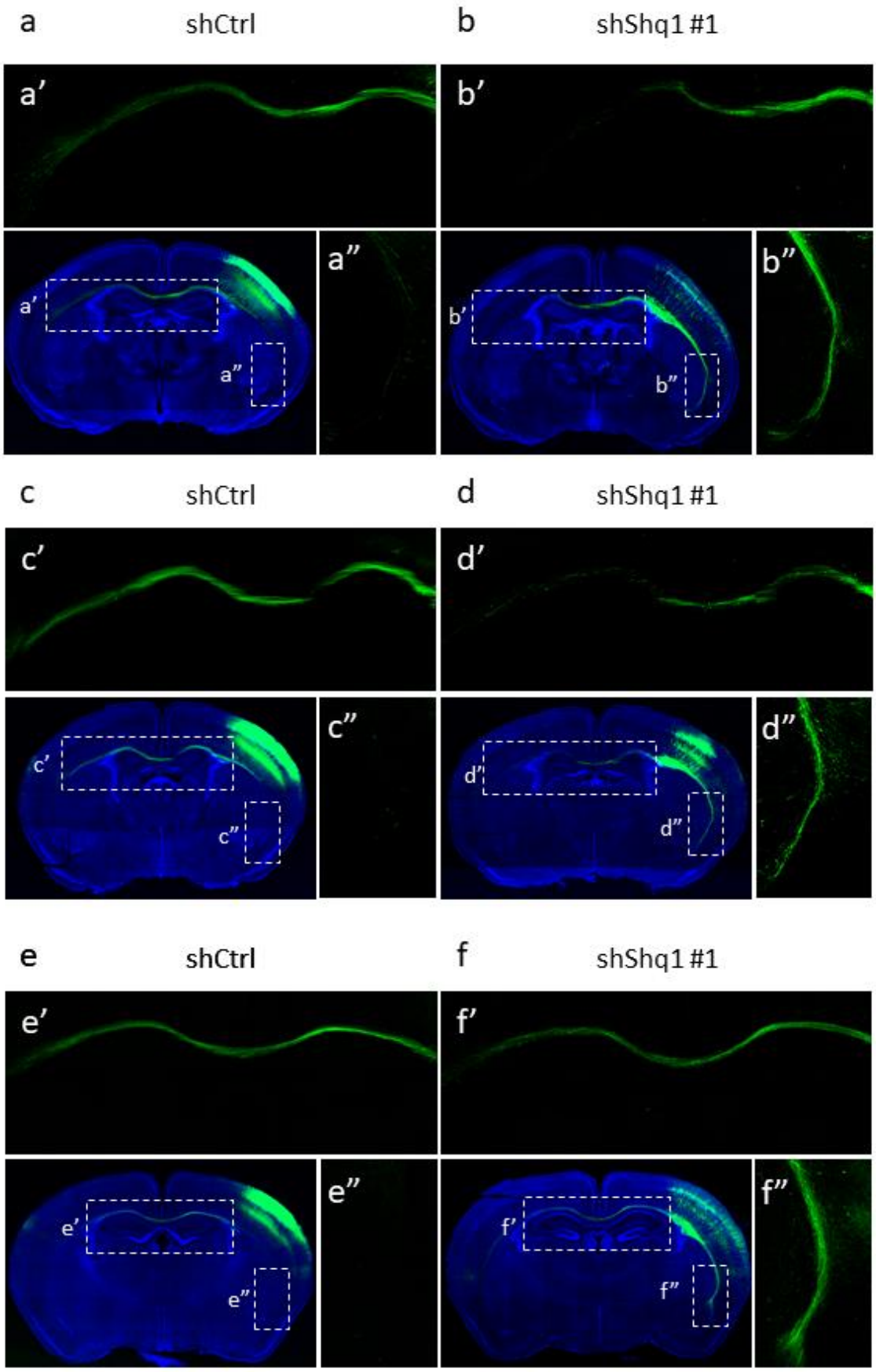
a
shCtrl
b
shShq1 #1
a'
b'
a''
b''
c
shCtrl
d
shShq1 #1
c'
d'
c''
d''
e
shCtrl
f
shShq1 #1
e'
f'
e''
f''

Figure 8. Shq1 KD may altered cortical projection. (a)(c)(e) Whole brain and zoomed images of brains electroporated with shCtrl at P7, P14, and P21 respectively. The majority of GFP+ cells projected axons to contralateral cortex through corpus callosum. DAPI (blue) was used for nucleic acid staining. (b)(d)(f) Whole brain and zoomed images of brains electroporated with shShq1#1 at P7, P14, and P21 respectively. GFP+ cells extended their axons laterally towards the external capsule or/and projected their axons to contralateral cortex. DAPI (blue) was used for nucleic acid staining.

Figure 9

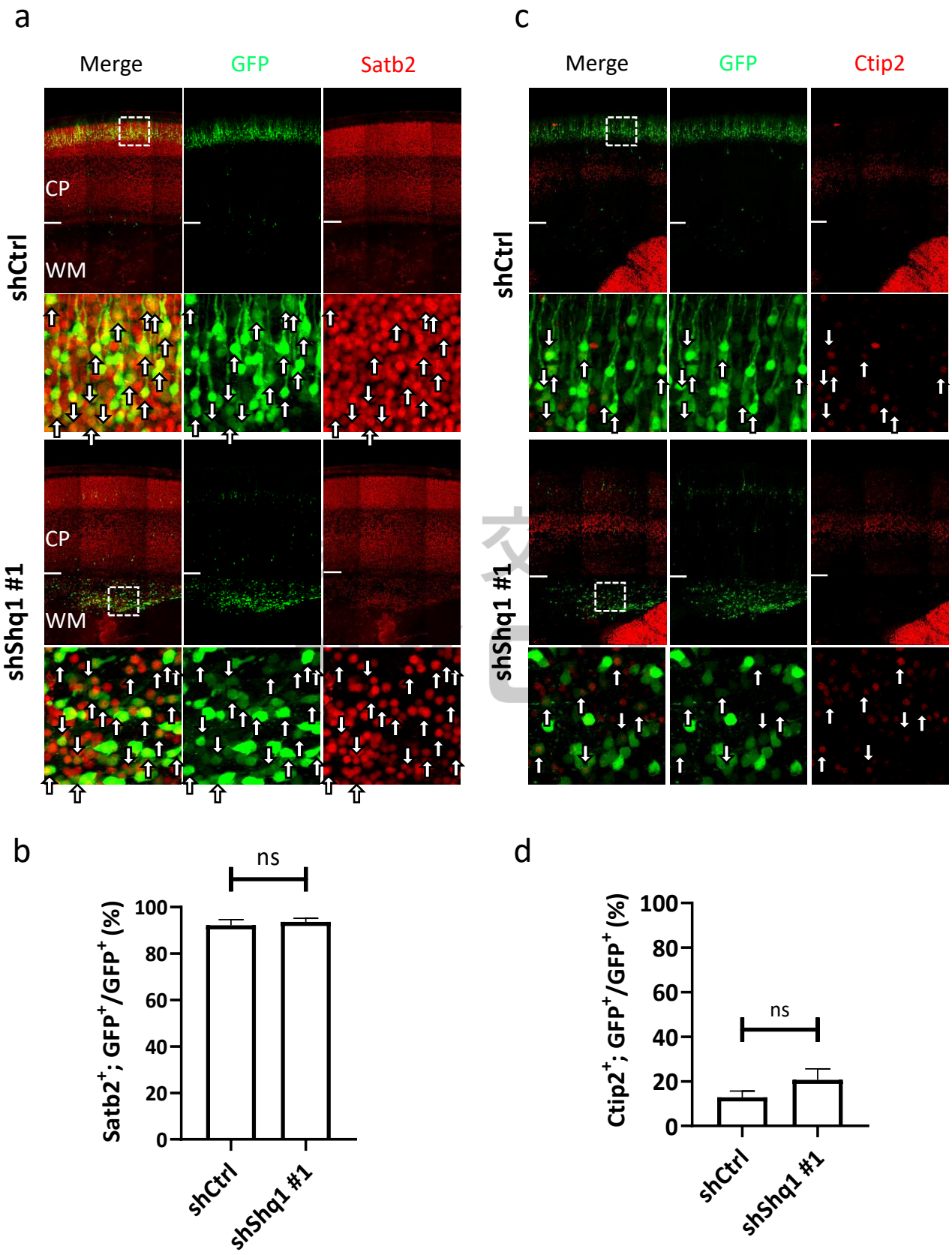
a
Merge
GFP
Satb2
shCtrl
shShq1 #1
CP
WM
c
Merge
GFP
Ctip2
shCtrl
shShq1 #1
b
ns
Satb2+; GFP+/GFP+ (%)
100
80
60
40
20
0
shCtrl
shShq1 #1
d
ns
Ctip2+; GFP+/GFP+ (%)
100
80
60
40
20
0
shCtrl
shShq1 #1

Figure 9. Shq1 KD cells may not change their cell fate. (a) Immunostaining of Satb2 (red) in brains electroporated with shCtrl and shShq1#1 at P7. The majority of GFP+ cells (~90%) expressed Satb2 in both control and KD brains. White arrows represented the colocalization of Satb2 and GFP signal. (b) Bar plot of the percentage of Satb2+ cells in brains electroporated with control or Shq1 shRNAs. shCtrl: N=3 mice; shShq1#1: N=3 mice. Error bar represented SEM. Welch's t tests. (c) Immunostaining of Ctip2 (red) in brains electroporated with shCtrl and shShq1#1 at P7. Only about 15% of GFP+ cells expressed Ctip2 in both control and KD brains. White arrows represented the colocalization of Ctip2 and GFP signal. (d) Bar plot of the percentage of Ctip2+ cells in brains electroporated with control or Shq1 shRNAs. shCtrl: N=3 mice; shShq1#1: N=3 mice. Error bar represented SEM. Welch's t tests.

Figure 10

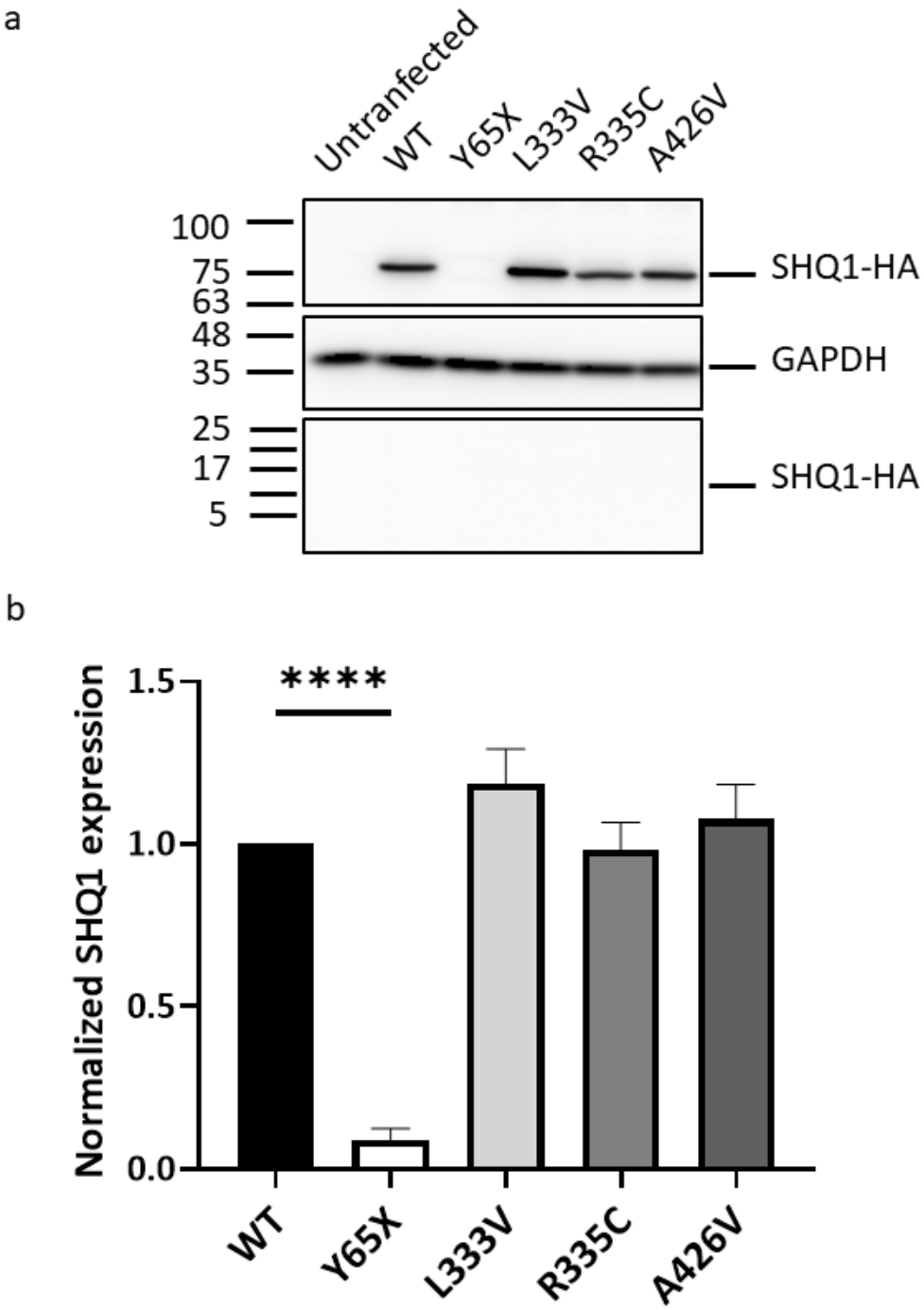
a
Untranfected
WT
Y65X
L333V
R335C
A426V
100
75
63
48
35
25
17
5
SHQ1-HA
GAPDH
SHQ1-HA
b
Normalized SHQ1 expression
1.5
1.0
0.5
0.0
****
WT
Y65X
L333V
R335C
A426V

Figure 10. The protein expression of different SHQ1 variants. (a) Western blot of SHQ1 expression in HEK293T cells transfected with SHQ1 variants. Y65X expression nearly disappear in transfected cells. However, the protein levels of L333V, R335C, and A426V were no difference compared to WT SHQ1. (b) Bar plot of the expression of SHQ1 in cells transfected with SHQ1 variants. N=3 in each group. Error bar represented SEM. Ordinary one-way ANOVA. ****p<0.0001

Figure 11

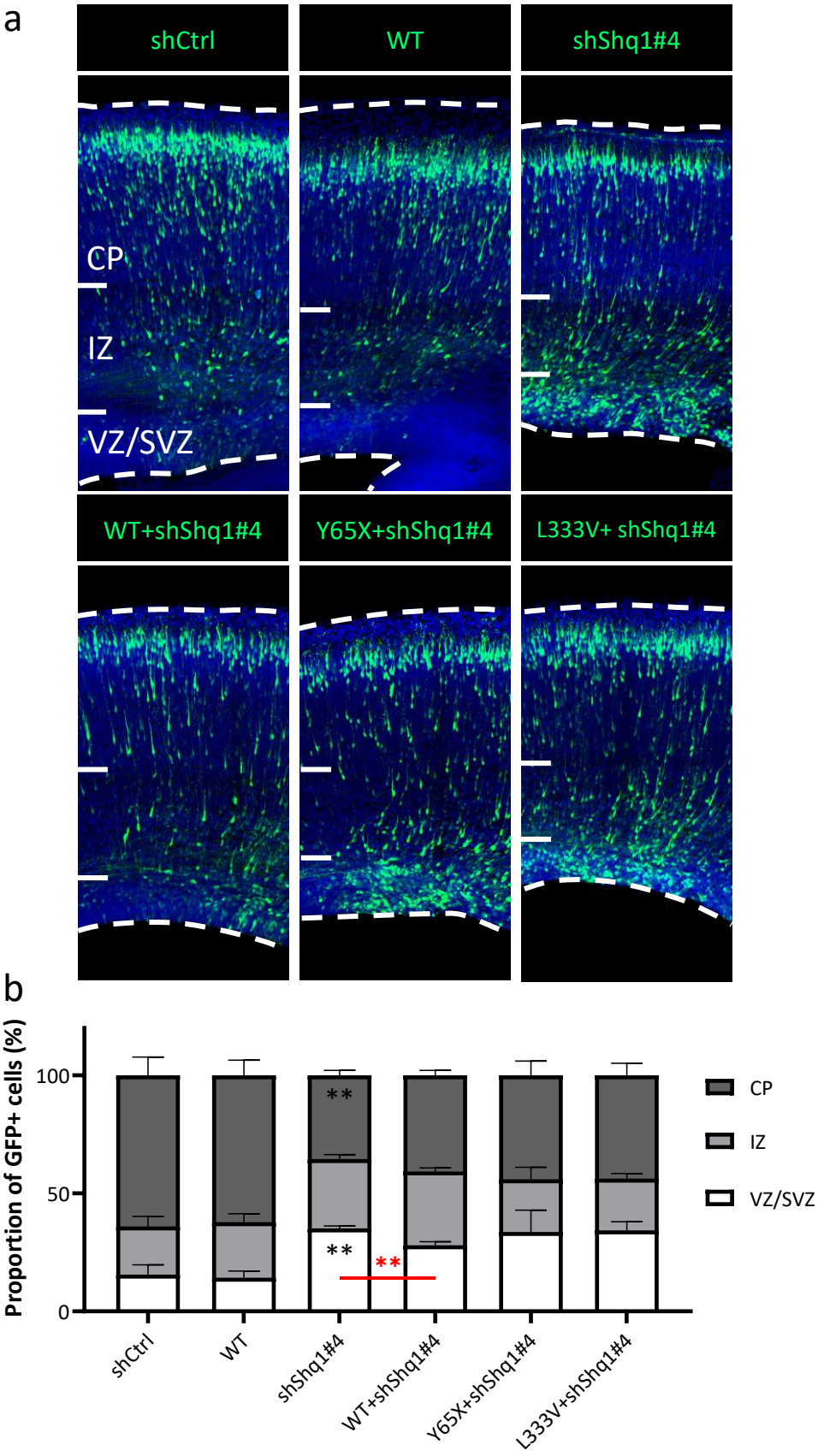
a
shCtrl
WT
shShq1#4
CP
IZ
VZ/SVZ
WT+shShq1#4
Y65X+shShq1#4
L333V+ shShq1#4
b
Proportion of GFP+ cells (%)
100
50
0
**
**
**
CP
IZ
VZ/SVZ
shCtrl
WT
shShq1#4
WT+shShq1#4
Y65X+shShq1#4
L333V+shShq1#4

Figure 11. SHQ1 variants failed to rescue the abnormal cell distribution caused by Shq1 KD. (a) Cell distributions of brains electroporated with shCtrl, SHQ1 WT cDNA, shShq1#4, or SHQ1 variants along with shShq1#4 at E18.5. In brains electroporated with Y65X or L333V along with shShq1#4, most GFP+ cells remained in IZ and SVZ. DAPI (blue) was used for nucleic acid staining. (b) Bar plot of cell distributions in brains electroporated shCtrl, SHQ1 WT cDNA, shShq1#4, or SHQ1 variants along with shShq1#4. shCtrl: N=7 mice; WT: N=2 mice; shShq1#4: N=6 mice; WT+shShq1#4: N=5 mice; Y65X+shShq1#4: N=3 mice; L333V+shShq1#4: N=3 mice. Error bar represented SEM. Brown-Forsythe and Welch ANOVA tests. Black asterisks compared the marked bars to shCtrl. Red asterisks compared the two indicated bars. **p<0.01

Figure 12

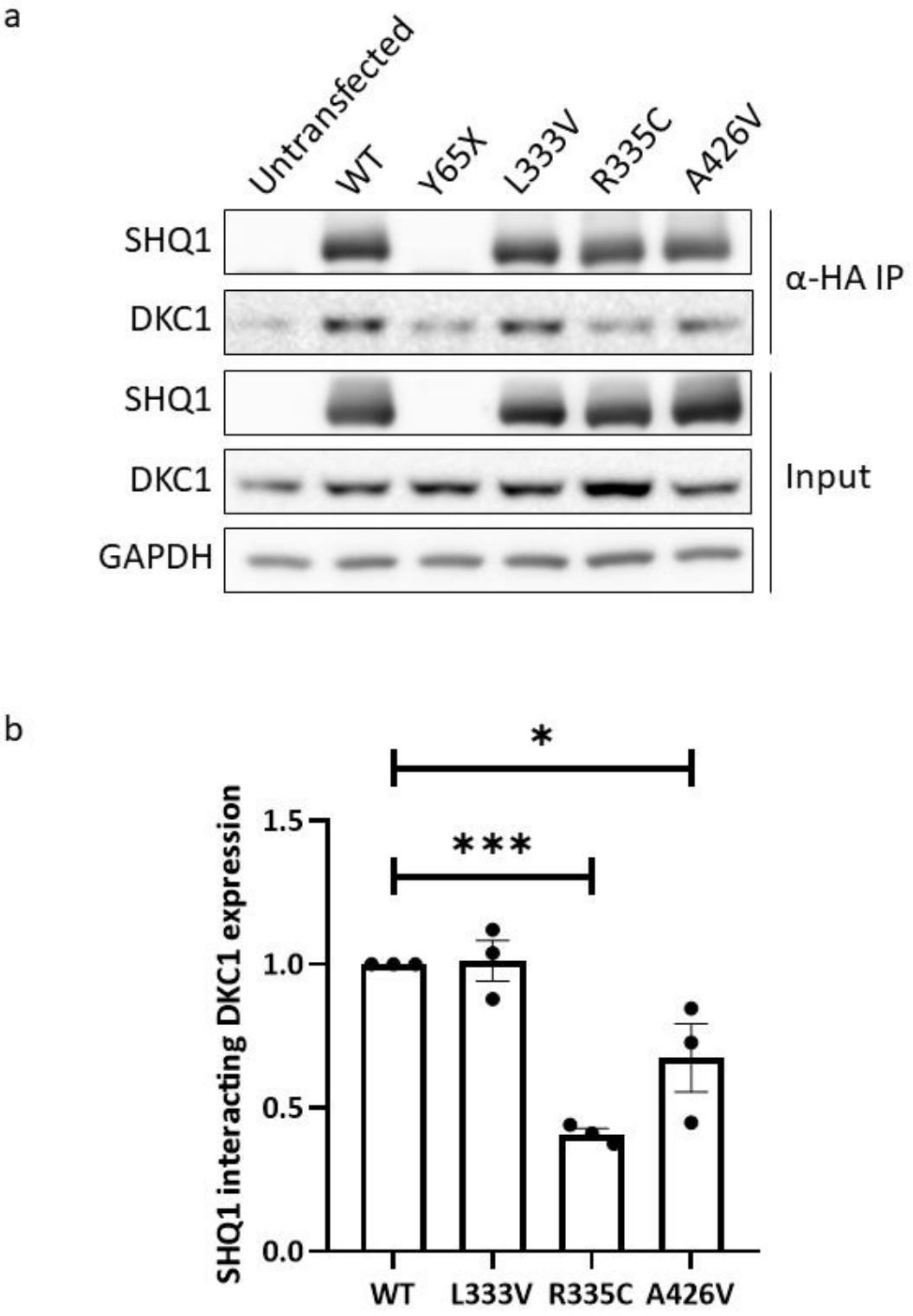
a
Untransfected
WT
Y65X
L333V
R335C
A426V
SHQ1
DKC1
α-HA IP
SHQ1
DKC1
GAPDH
Input
b
*
***
SHQ1 interacting DKC1 expression
1.5
1.0
0.5
0.0
WT
L333V
R335C
A426V

Figure 12. Most SHQ1 variants failed to bind with DKC1. (a) Co-immunoprecipitation of HA-tagged SHQ1 variants and endogenous DKC1 showed that SHQ1 interaction to DKC1 was significantly reduced in cells transfected with R335C and A426V variants compared to WT. However, there were no differences between cells expressing WT and L333V variant. (c) Bar plot of the expression of SHQ1 interacting DKC1 in different SHQ1 variants. N=3 in each group. Error bar represented SEM. Ordinary one-way ANOVA. *p<0.05, ***p<0.001